JCB Journal of Cell Biology

ARTICLE

Giant ankyrin-B suppresses stochastic collateral axon branching through direct interaction with microtubules

Keyu Chen[1,2*], Rui Yang[3*], Yubing Li[1], Jin Chuan Zhou[1,4], and Mingjie Zhang[1,2,4]

Giant ankyrin-B (gAnkB) is a 440-kD neurospecific ankyrin-B isoform and a high-confidence target for autism mutations. gAnkB suppresses axon branching through coordination of cortical microtubules, and autism-related mutation of gAnkB results in ectopic neuronal connectivity. We identified a bipartite motif from gAnkB, which bundles and avidly binds to microtubules in vitro. This motif is composed of a module of 15 tandem repeats followed by a short, conserved fragment also found in giant ankyrin-G (BG-box). Combination of these two parts synergistically increases microtubule-binding avidity. Transfection of astrocytes (which lack gAnkB) with WT gAnkB resulted in prominent bundling of microtubules, which did not occur with mutant gAnkB with impaired microtubule-binding activity. Similarly, rescue of gAnkB-deficient neurons with WT gAnkB suppressed axonal branching and invasion of EB3-tagged microtubules into filopodia, which did not occur with the same mutant gAnkB. Together, these findings demonstrate that gAnkB suppresses axon collateral branching and prevents microtubule invasion of nascent axon branches through direct interaction with microtubules.

Introduction

Axons are capable of forming collateral branches, which expand neural connectivity >1,000-fold, provide a mechanism for plasticity, and promote neuroregeneration following injury (Armijo-Weingart and Gallo, 2017; Kalil and Dent, 2014; Menon and Gupton, 2018). Axon bifurcations begin with actin-dependent filopodial extensions, which are subsequently invaded and stabilized by microtubules (MTs; Dent et al., 1999; Kalil and Dent, 2014; Yu et al., 1994). Multiple MT-associated proteins normally prevent entry of MTs into filopodia and function in vivo to suppress ectopic axonal branches (Bouquet et al., 2004; Homma et al., 2003; Qiang et al., 2006; Tymanskyj et al., 2017; Yu et al., 1994). Local regulation of the protein interactions of axonal MTs thus can determine whether a nascent filopodium will mature into a full-fledged axon branch.

Giant ankyrin-B (gAnkB) is a 440-kD neurospecific ankyrin-B isoform associated with axonal plasma membranes through binding to L1 cell adhesion molecule (L1CAM), which has recently been reported to repress axon branching (Bennett and Lorenzo, 2016; Yang et al., 2019). gAnkB is encoded by *ANK2*, which is a high-confidence autism spectrum disorder (ASD) gene, and several de novo ASD mutations target the neural specific domain (NSD) of gAnkB (De Rubeis et al., 2014; Iossifov et al., 2014; Yang et al., 2019). Interestingly, a mouse model for a human ASD-associated frameshift mutation in the neurospecific giant exon of gAnkB exhibits phenotypes consistent with increased axon branching that include ectopic structural connectivity as well as increased numbers of excitatory synapses (Yang et al., 2019). Cultured neurons from these gAnkB mutant mice exhibit increased axonal branching as well as increased invasion of MTs into axonal filopodia (Yang et al., 2019). Moreover, EM revealed displacement of cortical MTs away from the plasma membrane in axons of gAnkB frameshift mutant mice, as well as in L1CAM Y1229H mutant mice, where L1CAM lacks gAnkB-binding activity (Yang et al., 2019). These findings suggest that gAnkB represses axonal branching through interaction with cortical MTs, either directly or indirectly through intermediary protein(s), and that loss of this activity contributes to autism.

This study addresses the related questions of how gAnkB interacts with MTs and whether gAnkB requires MT association to repress axonal branching. Ankyrin-B was previously reported

[1]Division of Life Science, State Key Laboratory of Molecular Neuroscience, Hong Kong University of Science and Technology, Clear Water Bay, Kowloon, Hong Kong, China; [2]Greater Bay Biomedical Innocenter, Shenzhen Bay Laboratory, Shenzhen, China; [3]Department of Biochemistry, Duke University Medical Center, Durham, NC; [4]Center of Systems Biology and Human Health, Hong Kong University of Science and Technology, Clear Water Bay, Kowloon, Hong Kong, China.

*These authors contributed equally to this work; Correspondence to: Mingjie Zhang: mzhang@ust.hk; Rui Yang: yangruisz@gmail.com; R. Yang's present address is Department of Genetics, Yale University School of Medicine, New Haven, CT.

to associate with MTs in in vitro assays through its ANK repeat domain, which is shared by both 220-kD AnkB and gAnkB polypeptides (Chan et al., 1993; Davis and Bennett, 1984; Davis et al., 1991; Kunimoto et al., 1991). However, levels of 220-kD AnkB are not reduced in a mouse model for human ASD frameshift mutation targeting gAnkB (Yang et al., 2019). In addition, neurons from mice that express 220-kD AnkB but lack gAnkB due to conditional loss of its giant neurospecific exon also exhibit increased axon branching and invasion of MTs into filopodia (Yang et al., 2019). Moreover, 220-kD AnkB is associated with intracellular synaptic cargos through binding to PIP3 phosphoinositides, while gAnkB is associated with L1CAM on axonal plasma membranes (Lorenzo et al., 2014; Yang et al., 2019). These considerations suggest that gAnkB contacts MTs through additional site(s) in its NSD that are not shared with 220-kD AnkB.

We report that gAnkB contains a bipartite MT-interaction site located in its NSD that confers strong MT-binding/bundling activity in cells. We further demonstrate that gAnkB requires its neurospecific MT-binding/bundling activity in order to repress ectopic axonal branching in cultured hippocampal neurons. These findings, together with earlier work, establish a molecular pathway required to suppress ectopic axon branches that connects axonal MTs to the plasma membrane through direct association with gAnkB, which in turn is linked to the plasma membrane by L1CAM.

Results

gAnkB represses axon branching and invasion of MT into axonal filopodia

We first sought to confirm the previously reported axonal localization of gAnkB and the role of gAnkB in axonal branching (Chan et al., 1993; Yang et al., 2019). 440-kD gAnkB has an NSD encoded by a single 8-kb exon (exon 37) acquired early in vertebrate evolution that is inserted between the spectrin-binding domain (SBD) and the death domain (DD; Figs. 1 A and 2 A). Costaining of cultured day 4 in vitro (DIV4) hippocampal neurons with a sheep pan antibody that recognizes the C-terminal shared region of both isoforms and a rabbit antibody that recognizes the gAnkB neural specific region confirmed that the subcellular distribution of gAnkB is mostly limited to axons, whereas 220-kD AnkB is present in both axons and dendrites (Fig. 1 B; Lorenzo et al., 2014). To determine effects of gAnkB deficiency on axon branching, we employed a gAnkB-specific conditional knockout mouse (*AB37*$^{f/f}$), where exon 37, which encodes the NSD, was flanked with two loxP sites (Fig. S1 A; Yang et al., 2019). By crossing these mice with mice expressing Cre-recombinase under control of the Nestin promoter, the expression of gAnkB was disrupted in over 90% of the neurons (Fig. S1 B; Yang et al., 2019). Cultured hippocampal neurons from *AB37*$^{f/f}$ *Nes-Cre*$^{+}$ mice showed a significantly increased number of axon branches compared with neurons from WT mice (*AB37*$^{f/f}$ *Nes-Cre*$^{-}$ = 0.6 ± 0.07 branches/100 µm; *AB37*$^{f/f}$ *Nes-Cre*$^{+}$ = 1.6 ± 0.1 branches/100 µm; Fig. 1 C), which is consistent with findings in neurons from a mouse model bearing *ANK2* human ASD-related mutations (Yang et al., 2019). Thus, we establish that gAnkB is selectively located in axons and that neurons lacking gAnkB form more axon branches.

Neurons from mouse models bearing human *ANK2* ASD-related mutations targeting gAnkB or L1CAM-Y1229H mutation eliminating L1CAM ankyrin-binding activity exhibit increased frequency of MT invasion into filopodia formed on the axonal shaft (Yang et al., 2019). To determine how the MT dynamics change in axons of *AB37*$^{f/f}$ *Nes-Cre*$^{+}$ neurons lacking gAnkB, we time-lapse imaged neurons transfected with MT end-binding protein fused with fluorescent protein tandem Tomato (EB3-tdTM), which binds to the growing MT plus ends to form a "comet" (Akhmanova and Steinmetz, 2008; Kleele et al., 2014). In neurons from WT mice (*AB37*$^{f/f}$ *Nes-Cre*$^{-}$), EB3 comets uniformly moved toward the distal end of axons (Video 1). Over a 2-min recording period, the majority of EB3 comets remained in the axon shaft, as illustrated by the stacking images over the time period (Fig. 1 D, top left). In neurons from *AB37*$^{f/f}$ *Nes-Cre*$^{+}$ mice, EB3 comet movement deviated from the axon shaft direction with higher frequency, which was illustrated by the stacking images over time (Fig. 1 D, top right; and Video 2). We termed this kind of comet as a "nonaxis comet." The number of nonaxis EB3 comets in neurons from *AB37*$^{f/f}$ *Nes-Cre*$^{+}$ mice (1.98 ± 0.28 comets/100 µm/2 min; n = 10) was significantly (P = 0.0024; unpaired t test) higher than in *AB37*$^{f/f}$ *Nes-Cre*$^{-}$ neurons (0.75 ± 0.21 comets/100 µm/2 min; n = 10; Fig. 1 D). In addition, some EB3 comets that deviated from the axonal shaft further invaded into axonal filopodia to stabilize nascent collateral axon branches (Fig. 1 D and Video 3), which is more frequent in gAnkB-deficient neurons (*AB37*$^{f/f}$ *Nes-Cre*$^{-}$ neuron is 0.76 ± 0.21 comets/100 µm/2 min; *AB37*$^{f/f}$ *Nes-Cre*$^{+}$ neuron is 1.67 ± 0.26 comets/100 µm/2 min; n = 10; P = 0.016; unpaired t test; Fig. 1 D and Video 4). Together, these results confirmed the function of gAnkB in suppressing axon branching and invasion of MTs into filopodia.

Identification of a gAnkB MT-binding/bundling site

We next evaluated the hypothesis that gAnkB directly interacts with MTs through its NSD. Because this ∼2,000-residue NSD (aa 1477–3561) is predicted to be intrinsically disordered (see Fig. S3 A), we divided it into six fragments (F1–F6: aa 1477–1792, 1793–2070, 2071–2375, 2376–2791, 2792–3188, and 3189–3561) according to sequence conservation among different species and secondary structure prediction (Fig. 2 A). These six fragments were expressed and purified as thioredoxin (Trx)-fused recombinant proteins in *Escherichia coli* and then evaluated for their binding to MTs using a cosedimentation assay with prepolymerized tubulins (Fig. 2 B). After ultracentrifugation under conditions that sediment MTs, proteins binding to MTs copellet with MTs and non–MT-bound proteins remain in the supernatant. Strikingly, F2 (gAnkB-F2; aa 1793–2070; note that the Trx tag was removed because the Trx-F2 band would overlap with the tubulin band) showed a very strong MT-binding activity, where all the gAnkB-F2 polypeptide copelleted with tubulin and no protein remained in the supernatant (Fig. 2 B). F1 (aa 1477–1792) showed some level of association with MTs, but the affinity was weaker than gAnkB-F2, with a smaller fraction copelleting with MTs (Fig. 2 B). The other four fragments did not

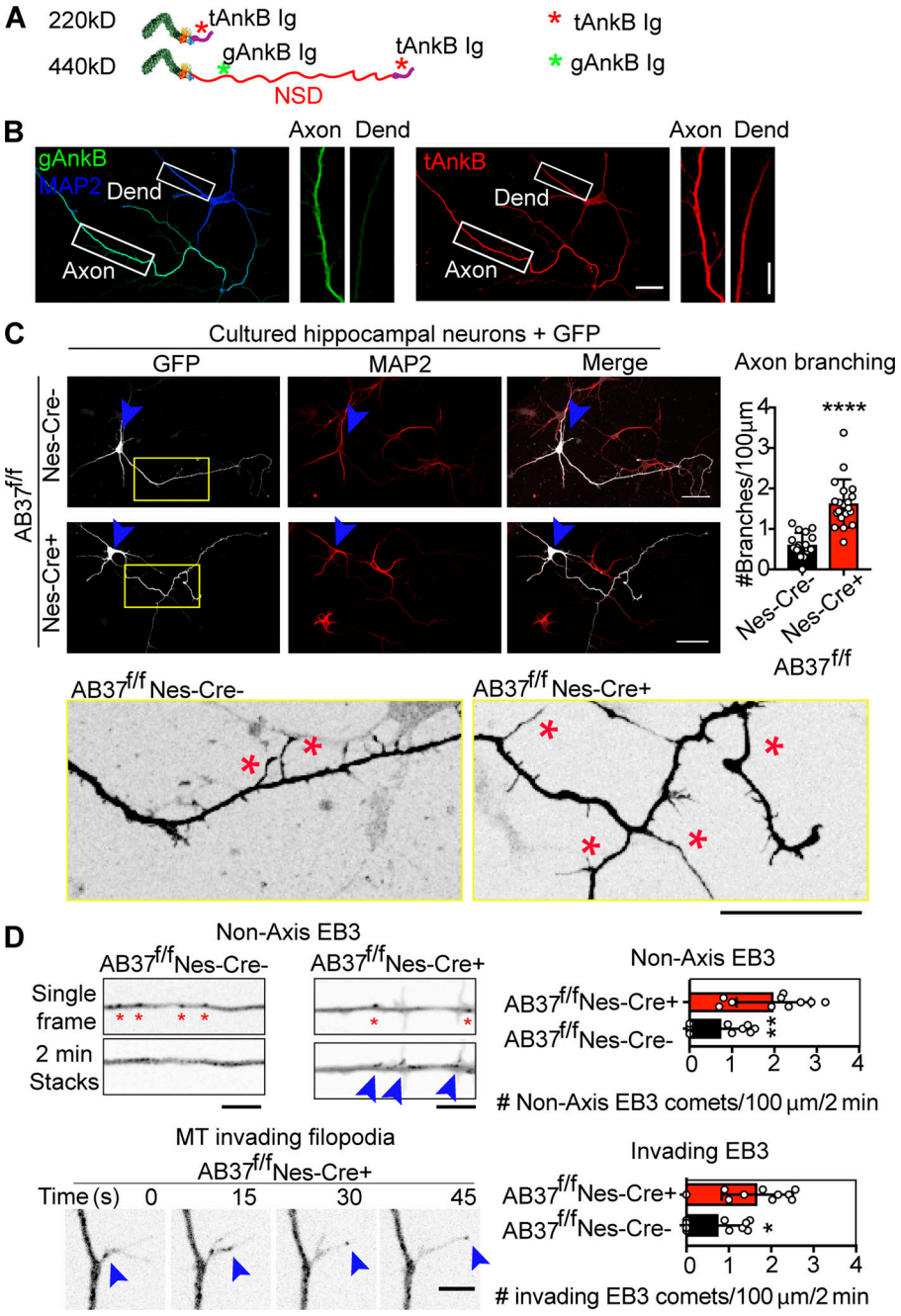

Figure 1. **gAnkB suppresses axon branching through regulating axonal MT dynamics.** **(A)** Schematic of 220-kD AnkB and 440-kD gAnkB. Asterisks indicate the binding sites of antibody against total AnkB (tAnkB Ig) or giant AnkB (gAnkB Ig). NSD is highlighted in red. **(B)** Fluorescence images of DIV4 cultured hippocampal neurons stained with gAnkB Ig (green), tAnkB Ig (red), and dendritic marker MAP2 (Dend; blue). A merged picture of gAnkB (green) and MAP2 (blue) staining is displayed on the left panel with high-magnification pictures of axon or dendrite for gAnkB staining to the right. The same neuron stained with tAnkB (red) is displayed in the right panel with high-magnification images of axon or dendrite for tAnkB staining to the right. (scale bar, 50 μm for whole neuron images; 5 μm for axon/dendrite high-magnification images). **(C)** Cultured hippocampal neurons from *AB37$^{f/f}$ Nes-Cre^{-}* (WT, top) or *AB37$^{f/f}$ Nes-Cre^{+}* (bottom) mice were transfected with GFP at DIV3 and fixed, then stained for MAP2 at DIV4. Blue arrowheads point to the cell body of the transfected neurons (scale bar, 50 μm). A zoomed-in image of the yellow-boxed axon region is displayed below for better visualization of branches (marked with red asterisks; scale bar, 50 μm). The number of branches longer than 10 μm is quantified (mean ± SEM; ****P < 0.0001, *t* test; *n* = 17 for WT; *n* = 20 for *AB37$^{f/f}$ Nes-Cre^{+}* from three biological replicates). **(D)** Top left: A single-frame image and a stacked 2-min time-lapse series image of an axon from an *AB37$^{f/f}$ Nes-Cre^{-}* neuron (Video 1) or an *AB37$^{f/f}$ Nes-Cre^{+}* neuron (Video 2; EB3-tdTM transfected, DIV4; scale bar, 5 μm). Red asterisks indicate EB3 comets and blue arrowheads indicate nonaxis EB3 comets. Nonaxis EB3 comet means the EB3 comet's moving direction deviated from the axis direction of the axon. Bottom left: The steps of MT invasion into a newly formed filopodium in the axon shaft of *AB37$^{f/f}$ Nes-Cre^{+}* neurons (Video 3; scale bar, 5 μm). Blue arrowheads track the movement of one EB3 comet. Right: Quantification of the number of nonaxis EB3 comets or the number of invading (into filopodia) EB3 comets (mean ± SEM; *t* test; **P = 0.0024 for nonaxis EB3; *P = 0.016 for invading EB3; *n* = 10 cells in all conditions from three biological replicates).

copellet with MTs (Fig. 2 B). Similarly, as a negative control, the gAnkB C-terminal domain (CD; aa 3748–3957), failed to cosediment with MTs (Fig. S4 A). Taken together, gAnkB-F2 is a major MT-binding site of gAnkB.

We employed an imaging-based assay to test the MT-bundling activity of gAnkB-F2. Prepolymerized tubulin (rhodamine labeled) was mixed with purified gAnkB-F2 (Alexa Fluor 488 labeled) and imaged by fluorescence microscopy. Strikingly, in the presence of gAnkB-F2, the originally short and thin single-MT filaments bundled together and formed very long and thick fascicles (Fig. 2 C, red; the MT filament or bundle width is quantified in Fig. 2 D; gAnkB-F2 group, 4.99 ± 0.47 μm; GFP control, 0.26 ± 0.01 μm). The gAnkB-F2 signal (green) perfectly colocalized with the bundled MTs (Fig. 2 C, red), and this phenomenon was not observed in the control sample, where purified GFP was mixed with prepolymerized tubulins (Fig. 2, C and D). In fact, after adding gAnkB-F2, prepolymerized tubulin solution immediately became turbid (Fig. 2 E). We then imaged MTs by negative staining EM (Fig. 2 F). In the presence of gAnkB-F2, MT filaments were well aligned in parallel and formed thick bundles (Fig. 2 F, right; the width is quantified in Fig. 2 G). In sharp contrast, in the absence of gAnkB-F2, the "naked" MTs were isolated and scrambled (Fig. 2 F, left; and Fig. 2 G). The distribution of distances between two neighboring aligned MTs in the gAnkB-F2 bundled MT fascicles centers on 4–6 nm (Fig. S3 C), which is shorter than the measurements of other MT-associated protein–bundled MT fascicles, such as INF2-FH1FH2 (10 to ~12 nm; Gaillard et al., 2011), MAP65-1 (~30

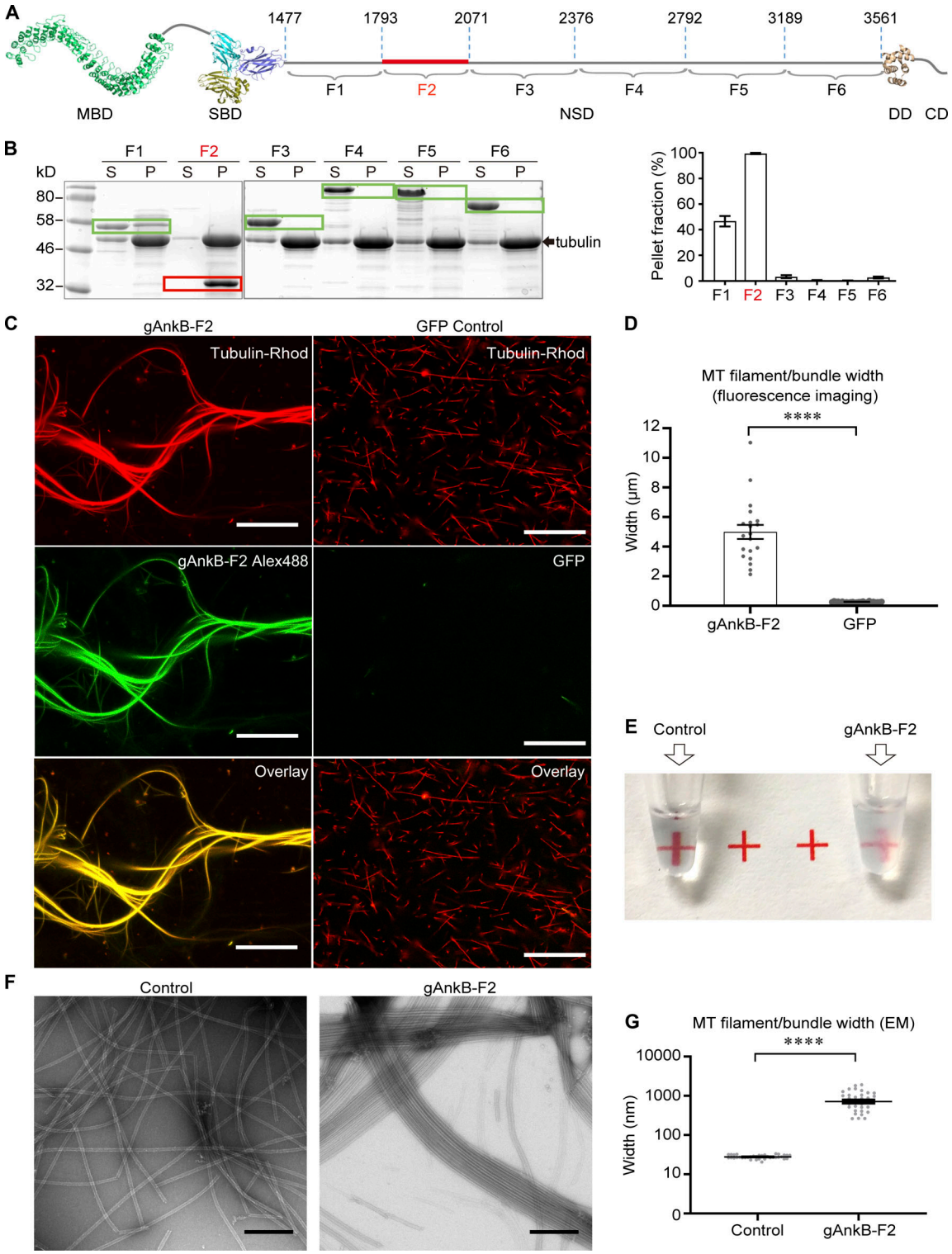

Figure 2. **A conserved and intrinsically disordered sequence in the NSD of gAnkB binds and bundles MTs. (A)** Domain organization of gAnkB illustrating the membrane binding domain (MBD), the SBD, the NSD spanning F1–F6, the DD, and the CD. Amino acid number labels the borders of the six small fragments (F1–F6) in the NSD used for the MT-binding assay. **(B)** Coomassie blue–stained SDS-PAGE gel of a MT cosedimentation experiment performed with 2 mg/ml polymerized tubulins and different gAnkB NSD fragments (F1–F6), each at 5 μM. Supernatant and pellet fractions are labeled as S and P, respectively. The bands of tubulin (~55 kD) are marked by an arrow. The bands for gAnkB fragments are indicated with red or green boxes. The fraction of gAnkB fragments present in the pellet were quantified on the basis of band intensity and SDS-PAGE sample loading ratio (right panel; mean ± SEM; data from three batches of repeat experiments). All gAnkB fragments contain a Trx tag (a fusion tag used in protein expression), except for F2, from which the Trx tag was removed. **(C)** Confocal images of in vitro Taxol-stabilized MTs (ratio of rhodamine [Rhod]-tubulin/unlabeled tubulin is ~8%; red) mixed with Alexa Fluor 488 (Alex488)–labeled gAnkB-F2 (green) or purified recombinant GFP (negative control). Scale bars, 30 μm. MT filament or bundle width quantification is shown in

D. **(D)** Measured MT filament or bundle width from C. Mean ± SEM; *t* test; ****P < 0.0001; *n* = 20 for gAnkB-F2; *n* = 25 for GFP group. **(E)** Comparison of prepolymerized tubulin heterodimer (18.2 µM) after adding reaction buffer (control) or purified gAnkB-F2 (20 µM). **(F)** Negative-stained EM images of free MTs (left) and gAnkB-F2 bundled MTs (right). Scale bars, 400 nm. **(G)** Measured MT filament or bundle width from EM images. y axis is logarithmic. Mean ± SEM; *t* test; ****P < 0.0001; *n* = 36 for control group; *n* = 52 for gAnkB-F2 group.

nm; Gaillard et al., 2008), and MAP65-4 (~15 nm; Fache et al., 2010). Taken together, gAnkB contains a stretch of amino acids (1793–2070) that avidly bind and bundle MTs in vitro.

A bipartite gAnkB MT-binding/bundling site

To further characterize how gAnkB-F2 binds to MTs, we analyzed the sequence features of gAnkB-F2. Interestingly, gAnkB-F2 contains 15 consecutive 12-residue (12-aa) imperfect repeats with unknown function (Chan et al., 1993; Otto et al., 1991; Fig. 3, A and B; and Fig. S2 B). The module of 15 consecutive 12-aa repeats is highly conserved in mammalian gAnkB genes. However, mammalian giant ankyrin-G (gAnkG), a close family member of gAnkB, and gAnkB in birds, amphibians, and fish contain only one such repeat (Fig. S2 A). In addition, gAnkB-F2 contains a 34-residue domain adjacent to the last repeat (corresponding to aa 1984–2017 of human gAnkB), which is highly conserved among all vertebrates as well as in gAnkG (referred to as the BG-box; Fig. 3, A and C; and Fig. S2 A). The sequence containing 15 12-aa repeats and the BG-box of gAnkB (aa 1806–2017; Fig. 3 A) is predicted to be disordered (Fig. S3 A, highlighted with a green box). Circular dichroism spectroscopy of the purified recombinant protein of gAnkB-F2 at a temperature range from 20 to 80°C revealed no evidence of secondary structure (Fig. S3 B). The 15 12-aa repeats of gAnkB are positively charged with a calculated isoelectric point of 10.6. These features of gAnkB are similar to other known nonmotor MT-associated proteins such as Tau, which interacts with MTs through positively charged, intrinsically disordered short repeats (Tortosa et al., 2016), though gAnkB-F2 and Tau share no aa sequence similarity.

To map the MT-binding site(s) of gAnkB-F2 in more detail, we generated four different polypeptides, each containing either 5 repeats (5R; aa 1793–1865), 10 repeats (10R; aa 1793–1924), 15 repeats (15R; aa 1793–1987), or the BG-box sequence (aa 1978–2070), respectively. The five-repeat polypeptide only weakly associated with MTs in the cosedimentation assay (Fig. 3 D). In contrast, the 10R and 15R proteins showed obvious MT-binding activity, with the 15R protein having a stronger affinity (Fig. 3 D). The BG-box of gAnkB also displayed MT-binding activity, although weaker than the 10R or 15R proteins (Fig. 3 D). Because the BG-box also exists in gAnkG, we tested the gAnkG fragment (aa 2193–2328) containing a BG-box and found that it can also bind to MTs (Fig. S4 B).

We next compared the MT-binding affinity of 15R without the BG-box and 15R with the BG-box (gAnkB-F2). The combination of 15R plus the BG-box dramatically enhanced the MT-binding affinity compared with 15R alone (Fig. 3 E, left). We further compared the MT-binding affinity between gAnkB-F2 and recombinant full-length Tau protein, which is a well-known MT-associated protein in axons and has strong MT-binding and MT-bundling activity in vitro (Kellogg et al., 2018; Scott et al., 1992). gAnkB-F2 displayed much stronger affinity than Tau when binding to prepolymerized tubulin heterodimers (Fig. 3 E, right). Taking these data together, we found that the combination of 15 12-aa repeats and a BG-box markedly enhanced the MT-binding affinity of the gAnkB-F2 polypeptide.

Full-length gAnkB bundles MTs in cells through 12-aa repeats

We next wanted to determine if full-length gAnkB interacts with MTs in cells, and, if so, whether this interaction is mediated by the neurospecific MT-binding site. As a first step, we performed structure–function studies in vitro to determine the critical region(s) required for MT bundling. We therefore compared the MT-bundling activities of the four gAnkB fragments (5R, 10R, 15R, and BG-box). Consistent with the MT cosedimentation–based binding assay (Fig. 3 D), MT-bundling activity is positively correlated with the number of repeats. The 5R protein showed no obvious MT-bundling activity (width = 0.46 ± 0.02 µm), and the fluorescence signal of Alexa Fluor 488–labeled gAnkB 5R polypeptide was faint and diffuse (Fig. 4). In contrast, the 15R polypeptide bundled MTs into a few very thick and long filaments (width = 2.56 ± 0.35 µm), and the fluorescence signal of gAnkB 15R was concomitantly enriched with the bundled MTs (Fig. 4). The 10R polypeptide was also able to bundle MTs, but the bundled MTs were thinner (filament width = 0.93 ± 0.06 µm) and shorter than those bundled by the 15R polypeptide (Fig. 4). Also, three short gAnkB fragments (repeats 1–5, 6–10, and 11–15, each containing five repeats) show similar bundling activity (Fig. S3 D, left), and two longer fragments (repeats 1–10 and 6–15, each containing 10 repeats) also display similar bundling activity (Fig. S3 D, right). This suggests that the number of repeats in gAnkB positively correlates with its MT-binding/bundling ability. It is further noted that the 10R and 15R gAnkB polypeptides uniformly decorate the entire unbundled MT filaments (Fig. 4), indicating that the gAnkB repeats bind to the entire MT tracks instead of preferentially clustering at the tips of MTs. Interestingly, although the BG-box showed distinct MT-binding activity, it exhibited very weak MT-bundling activity (width = 0.62 ± 0.03 µm; Fig. 4), where the frequency of bundled MTs as well as the thickness of bundled MTs was much less than the 10R and 15R polypeptides (Fig. 4).

We next determined the critical residues in the 12-residue motif of gAnkB that are required for MT binding and bundling. In previously reported cases of intrinsically disordered MT-binding proteins, charged residues are known to be important (Dehmelt and Halpain, 2005). Therefore, we substituted the conserved "Glu-Arg" cassette at the end of the 12-residue motif (indicated with triangles in Fig. 3 B and Fig. S5 A) with "Ala-Gly" in each of the 15 repeats (referred to as the "ER" mutation). Unexpectedly, this change has little effect on the MT-binding activity of gAnkB fragment (pellet fraction for 15R is 59.9% ± 12.6%; for 15R-ER, it is 57.7% ± 6.3%; Fig. S5 B). In another trial, three highly conserved residues in the third, fifth, and ninth

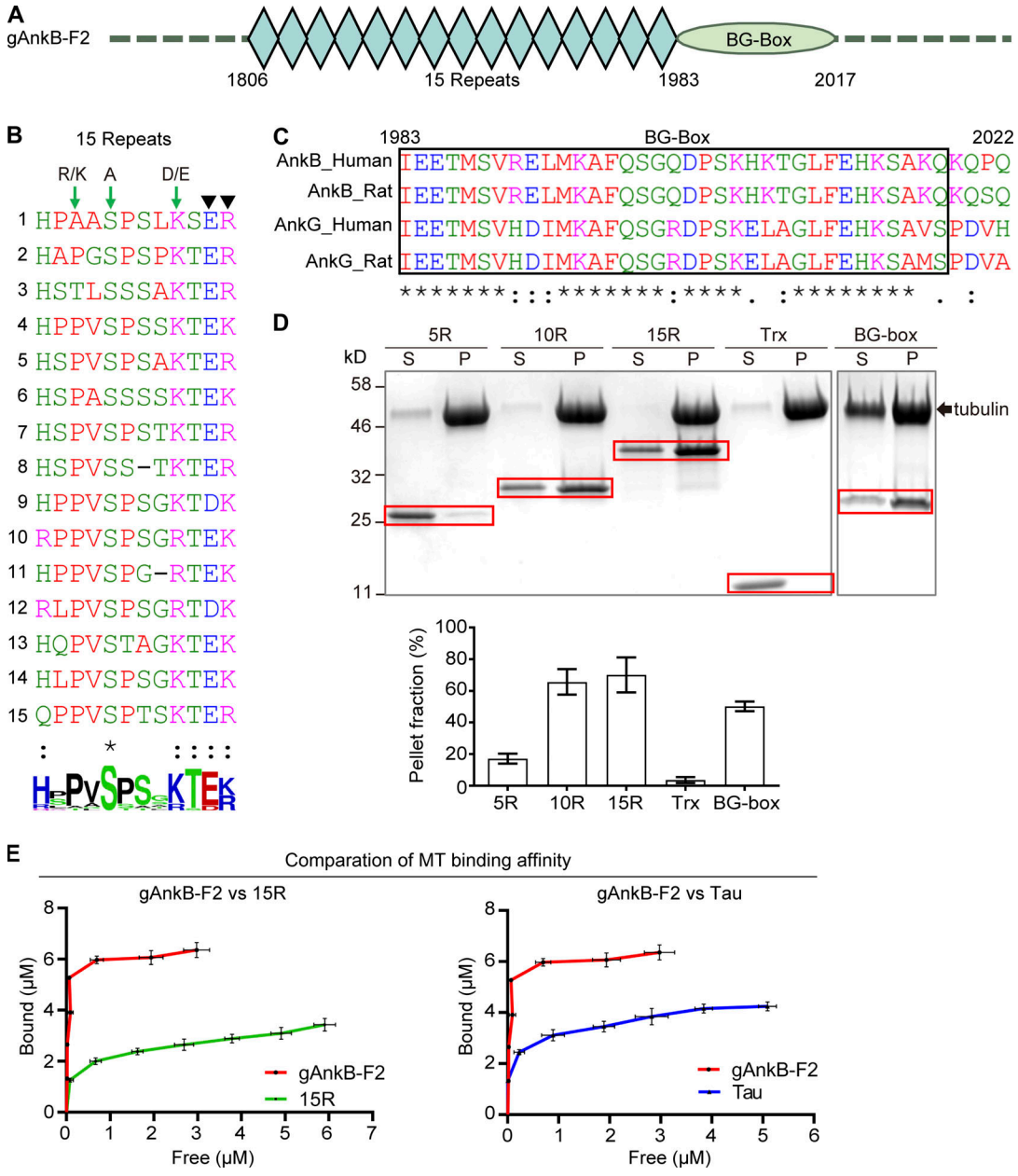

Figure 3. **The 15 tandem repeats and the BG-box together render gAnkB to bind and bundle MTs with high efficiency. (A)** Schematic of the gAnkB MT-binding domain (F2 in Fig. 2 A). Each blue diamond refers to a repeat (total of 15 consecutive repeats), and the green oval refers to a conserved motif shared by gAnkB and gAnkG (BG-box). **(B)** The aa sequence alignment of human gAnkB 15 12-aa repeats. An aa sequence logo plot is shown at the bottom of the alignment. Residues at the third, fifth, and ninth positions in the 12-aa repeats, marked by green arrows, are mutated in the PSK mutant of gAnkB. * and : indicate fully conserved and highly conserved residues, respectively. **(C)** The aa sequence alignment of BG-box of gAnkB and gAnkG from human or rat. The residue numbering corresponds to the human gAnkB sequence. *, :, and . indicate fully conserved, highly conserved, and conserved residues, respectively. **(D)** Coomassie blue–stained SDS-PAGE gel of a MT cosedimentation experiment performed with 5R (aa 1793–1865), 10R (aa 1793–1924), 15R (aa 1793–1987), gAnkB BG-box (BG-box; aa 1983–2070), and Trx (the fusion tag used in all of the AnkB fragments and used as a negative control). The tubulin bands (~55 kD) are indicated by an arrow. Percentages of proteins recovered from the MT-binding pellets were quantified on the basis of band intensity and SDS-PAGE sample loading ratio (mean ± SEM; n = 3). **(E)** Left: Saturation curves of gAnkB 15R (green; aa 1793–1987) or gAnkB 15R plus BG-box (gAnkB-F2, red; aa 1793–2070) binding to prepolymerized tubulins. Right: Saturation curves of gAnkB-F2 (red; aa 1793–2070; data are the same as in the left panel) or recombinant full-length human Tau protein (green) binding to prepolymerized tubulins. Gradient concentrations of proteins (gAnkB-F2, 15R or Tau in 2, 4, 6, 8, 10, 12, or 14 μM; 100 μl) were used in MT cosedimentation assays (final volume was 150 μl; tubulin concentration was 6 μM). The MT-bound fraction of each gAnkB fragment or Tau was calculated as the ratio of each protein recovered in pellet over the total input. Mean ± SEM in both x and y axes are displayed; n = 3.

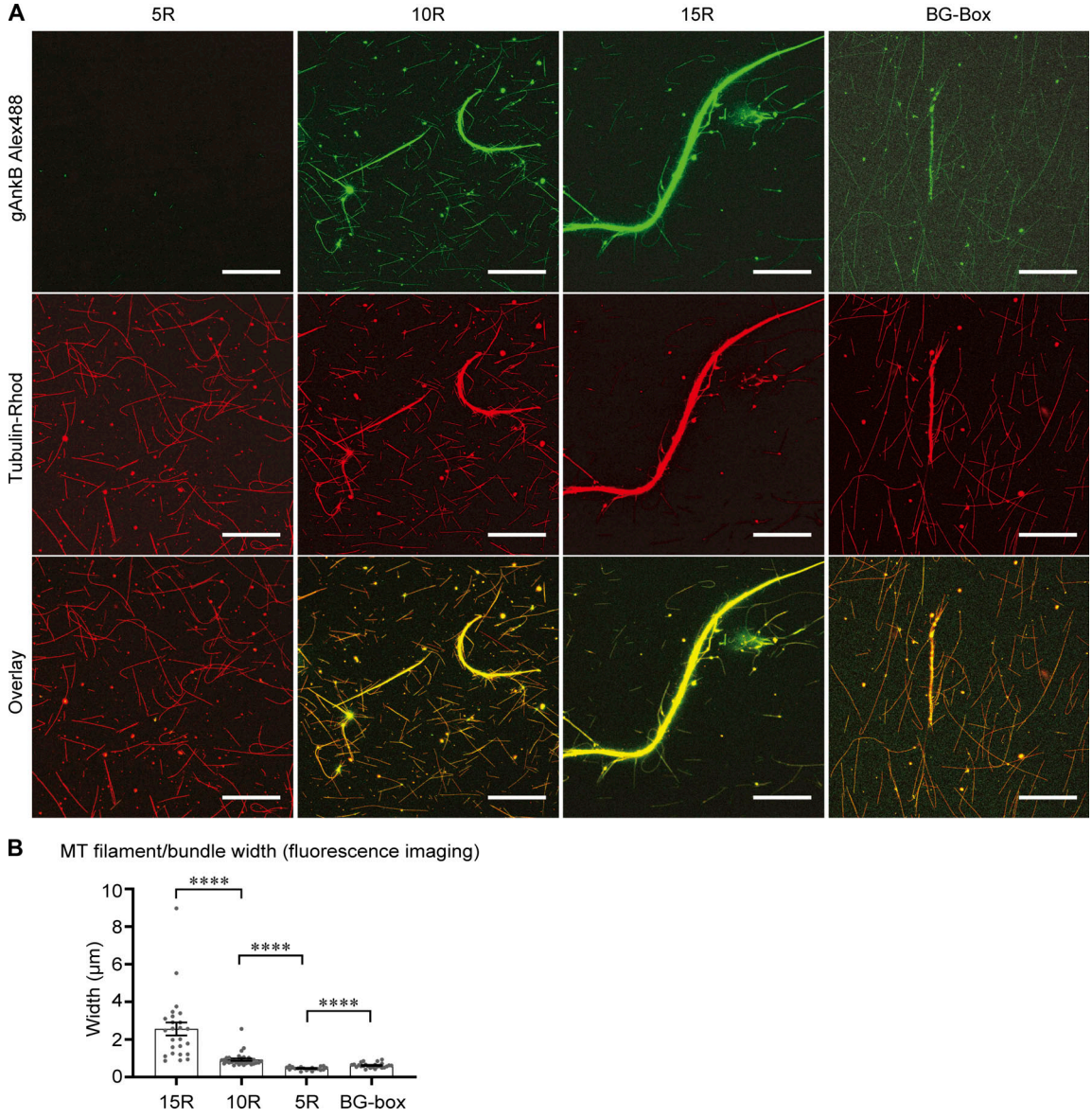

Figure 4. **gAnkB 15R contributes the major MT-bundling activity. (A)** Representative confocal microscopic images of in vitro Taxol-stabilized MTs (containing ∼8% rhodamine-labeled tubulin; red) mixed with fragments containing 5R, 10R, or 15R or BG-box (chemically labeled with Alexa Fluor 488 at ∼30%; green). Scale bars, 30 µm. **(B)** Quantification result of the MT filament or bundle width from in vitro MT-bundling assay fluorescence images. Mean ± SEM; ****P < 0.0001; *n* = 25 for 15R; *n* = 32 for 10R; *n* = 20 for 5R; *n* = 25 for BG-box. The Mann-Whitney test was used to compare 15R versus 10R and 10R versus 5R. The *t* test was used to compare 5R versus BG-box. Data derived from three individual experiments.

positions were mutated into Arg/Lys, Ala, and Asp/Glu, respectively, in all 15 repeats (referred to as the "PSK" mutant; Fig. 3 B, indicated by green arrows). The PSK mutation dramatically impaired MT-binding and MT-bundling activity of the 15R polypeptide, as revealed by cosedimentation assay (pellet fraction for 15R is 76% ± 2.2%; for 15R-PSK, it is 4.9% ± 0.7%) and fluorescence imaging–based assays (width = 2.33 ± 0.21 µm for 15R and 0.24 ± 0.01 µm for 15R-PSK), respectively (Fig. 5, A and B).

We next tested the effect of the PSK mutation in the context of full-length gAnkB polypeptide in cells. We employed an astrocyte-based cellular assay to evaluate the mutation's effect on MTs. The MT network of astrocytes is composed of randomly crossed single MTs (Fig. 5 C, left). The peak distribution of the diameter of MT bundles in nontransfected astrocytes is at 0.2-µm bin center (62%). We could also quantify the organization of MTs by measuring the angle between two neighboring MTs, where 0° refers to parallel and 90° refers to perpendicular arrangements of MTs, respectively. The peak distribution of the MT angles in nontransfected astrocytes is at 50° (11%) but is broader. When astrocytes were transfected with gAnkB cDNA (gAnkB-WT), the peak of the diameter of MT bundles increased to 0.3 µm (39%), and the angles between neighboring MTs are highly concentrated at the 10–15° window (53%; Fig. 5 C, middle). Because astrocytes lack endogenous expression of gAnkB (Yang et al., 2019), this change should be solely due to the

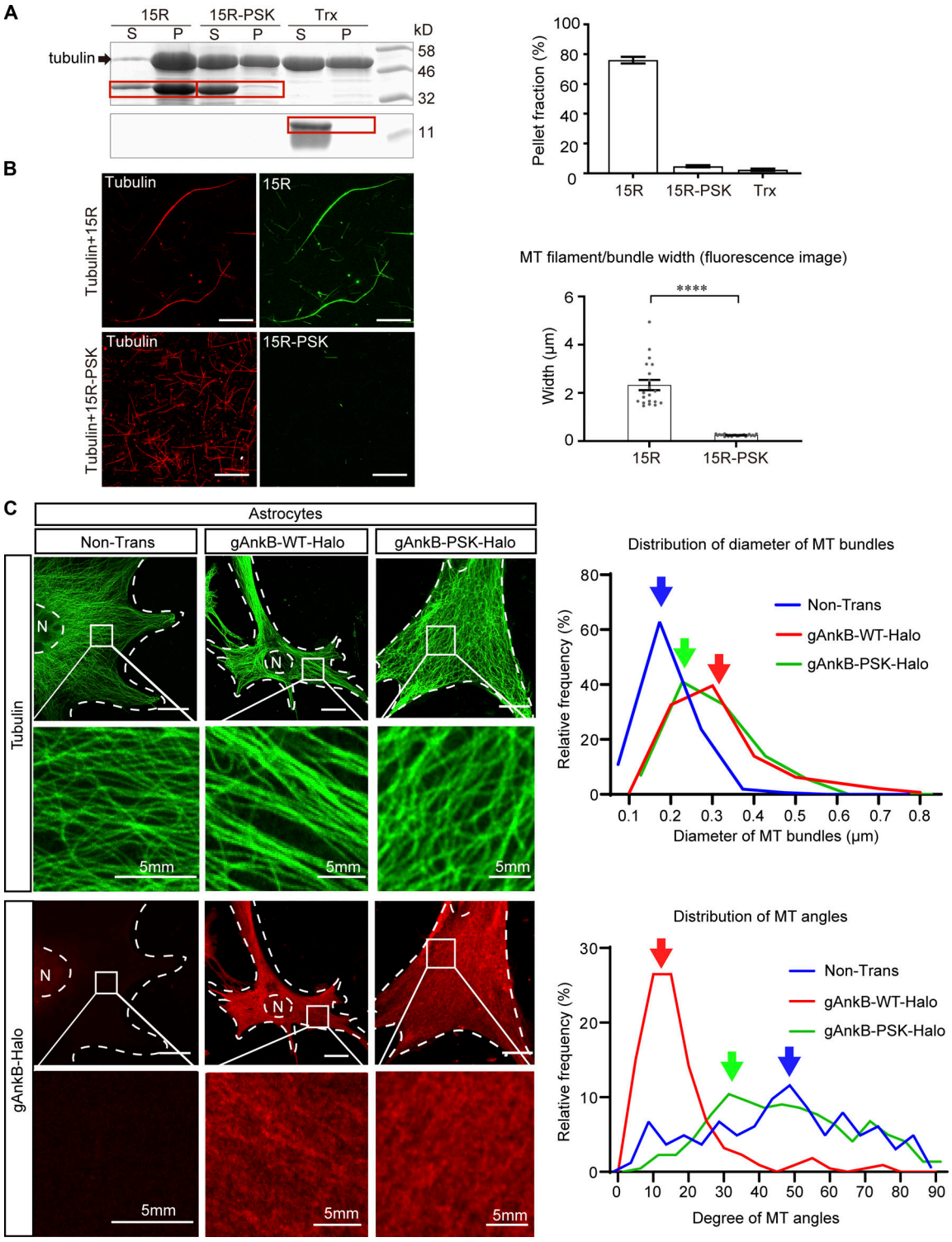

Figure 5. **Point mutations in the 15R segment impair MT-bundling activity of gAnkB. (A)** MT cosedimentation assay performed with the WT gAnkB 12-aa repeats (15R) or the PSK mutant of gAnkB 12-aa repeats (15R-PSK) with Trx as the control (each at 10 μM and Trx at 30 μM). The SDS-PAGE gel is shown in the left panel, and the percentage of proteins recovered from the MT-binding pellet fractions is shown in the right panel. Mean ± SEM; $n = 3$. **(B)** Confocal images of in vitro Taxol-stabilized MTs (contains ~8% rhodamine-labeled tubulin; red) mixed with WT gAnkB 15R (upper panel, labeled with Alexa Fluor 488; green) or the PSK mutant of gAnkB 15R (lower panel, labeled with Alexa Fluor 488; green). Scale bars, 30 μm. MT filament or bundle width quantification is presented in the right panel. Mean ± SEM; ****$P < 0.0001$; *t* test; $n = 20$ for 15R; and $n = 25$ for 15R-PSK. **(C)** Nontransfected astrocytes (left) and astrocytes transfected with gAnkB-WT-halo (middle) or gAnkB-PSK-halo (right) were fixed and stained with anti-tubulin antibody (green) and stained with Janelia Fluor 549 dye (red) after 24 h of expression (scale bars, 20 μm). Dashed lines indicate the borders of the astrocyte. The nuclear region is indicated with N. The histogram of the diameter and the angle of the MT bundle for all three conditions are displayed to the right (for diameter measurement, $n = 156$ for nontransfected; $n = 144$ for gAnkB-WT; $n = 136$ for gAnkB-PSK; for angle measurement, $n = 164$ for nontransfected; $n = 219$ for gAnkB-WT; $n = 221$ for gAnkB-PSK). Data were collected from 10 cells of three biological replicates. The arrowheads indicate the peak of distribution in each experimental group.

exogenously expressed gAnkB. This observation indicated that gAnkB promoted MT bundling in cells and that gAnkB also changed the pattern of MTs to a more parallel organization. Then, we introduced the PSK mutation into the full-length gAnkB cDNA (referred to as gAnkB-PSK). In gAnkB-PSK, the BG-box was not altered, because it is conserved through gAnkB and gAnkG, and changing this region may perturb other unknown functions shared by gAnkB and gAnkG. gAnkB-PSK mutant-transfected astrocytes exhibited reduced MT-bundling effect (40% of MT diameter peaked at 0.2 µm, bin center) compared with the gAnkB-WT–transfected cells (Fig. 5 C, right). Also, the angles of MTs showed a peak at 30°, again with a broad distribution (Fig. 5 C, right). The data in Fig. 5 suggested that the PSK mutation partially impaired the MT-bundling ability of gAnkB. We also checked the pattern of exogenously expressed gAnkB in astrocytes by adding Janelia Fluor 549 halo dye (gifted by Dr. Luke D. Lavis from Janelia Research Campus, Howard Hughes Medical Institute, Chevy Chase, MD), which labeled the halo tag fused to the C-terminus of full-length gAnkB. gAnkB-WT-halo displayed some copatterning with MT bundles, which is not obvious in gAnkB-PSK–transfected cells (Fig. 5 C, middle). The expression of gAnkB-WT-halo and gAnkB-PSK-halo was also confirmed in HEK293T cells with Western blot analysis (Fig. S1 D), showing that the WT and mutant gAnkB are expressed at comparable levels. Collectively, our data indicate that full-length gAnkB promotes MT bundling in astrocytes, largely through its 15 12-aa repeats.

gAnkB suppresses axon branching and MT invasion through its 12-aa repeats

To determine whether gAnkB MT-binding/bundling activity is required to suppress axon branching, we transfected either WT gAnkB-halo or gAnkB-halo containing the PSK mutation into DIV3 neurons from *AB37$^{f/f}$ Nes-Cre^{+}* mice and quantified axon branching at DIV4. We identified neurons expressing gAnkB polypeptides on the basis of labeling with halo dye. In Fig. 1, we showed that lack of gAnkB caused increased axon branches in neurons (Fig. 1 C). Neurons transfected with the gAnkB WT construct showed an obvious reduction of axon branching in *AB37$^{f/f}$ Nes-Cre^{+}* neurons (0.61 ± 0.08 branches/100 µm; n = 15; Fig. 6 A). Strikingly, gAnkB-PSK was totally incapable of rescuing the axon branching (1.8 ± 0.2 branches/100 µm; n = 18; Fig. 6 A), which indicates that the gAnkB 12-aa repeat–mediated binding to/bundling of MTs is required to suppress axon branching in hippocampal neurons.

Previously, we showed that lack of gAnkB caused more MTs to deviate from axonal shafts and invading into filopodia (Fig. 1 D). To test whether the 12-aa repeats was responsible for this function of gAnkB, we expressed gAnkB-WT-halo or gAnkB-PSK-halo in cultured hippocampal neurons from AB37$^{f/f}$ Nes-Cre^{+} mice and recorded the EB3 dynamics in their axonal shafts to see the rescue effect. The number of EB3 comets that deviated from the axonal shaft was smaller in gAnkB-WT than in gAnkB-PSK rescued neurons (Fig. 6 B, nonaxis EB3; 0.49 ± 0.21 comets/100 µm/2 min; n = 10 for gAnkB-WT; 1.78 ± 0.36 comets/100 µm/2 min; n = 10 for gAnkB-PSK; see Video 5 and Video 6 for gAnkB-WT and gAnkB-PSK rescue nonaxis EB3 comets in *AB37$^{f/f}$ Nes-Cre^{+}* neurons, respectively). Also, the frequency of EB3 comets that invaded into filopodia was lower in gAnkB-WT than in gAnkB-PSK rescued neurons (Fig. 6 B, invading EB3; 0.72 ± 0.31 comets/100 µm/2 min; n = 10 for gAnkB-WT; 1.65 ± 0.31 comets/100 µm/2 min; n = 10 for gAnkB-PSK; see Video 7 for gAnkB-PSK rescue invading EB3 comets in *AB37$^{f/f}$ Nes-Cre^{+}* neurons). Collectively, these data suggested that the MT-binding/bundling activity of the 12-aa repeats is required for full-length gAnkB to suppress axon branching through a direct interaction with MTs (Fig. 6 C).

Discussion

We identify a bipartite motif located in the NSD of gAnkB that bundles and avidly binds to MTs in vitro. This motif is comprised of a module of 15 tandem imperfect 12-aa repeats, conserved among eutherian and metatherian mammals but missing from gAnkG, followed by 34 residues, referred to as the BG-box, because this sequence is conserved between gAnkB and gAnkG. Although the 15R module is sufficient for MT binding and bundling, the combination of 15 12-aa repeats and BG-box resulted in a 16-fold increase in MT-binding avidity compared with 15R alone. Transfection of astrocytes (which lack gAnkB) with WT gAnkB resulted in prominent bundling of MTs, which did not occur with gAnkB bearing point mutations in the 15R module that impaired MT-binding activity. Similarly, rescue of gAnkB-deficient neurons with WT gAnkB suppressed axonal branching and invasion of EB3-tagged MTs into filopodia, which did not occur with mutant gAnkB with impaired MT-bundling activity. Together these findings demonstrate that gAnkB suppresses axon collateral branching and prevents MT invasion of nascent axon branches through direct interaction with MTs.

gAnkB is confined to the axonal plasma membrane, where it associates with L1CAM/neurofascin and is localized in periodic domains separated by 190 nm that are likely related to the spectrin-based periodic membrane skeleton (Xu et al., 2013; Zhong et al., 2014; Leterrier et al., 2015; Yang et al., 2019). gAnkB also preferentially interacts with cortical MTs via its large NSD, and removal of this domain from gAnkB leads to detachments of MTs from axonal plasma membranes (Yang et al., 2019). The functional consequences of coupling MTs through gAnkB to the periodic membrane skeleton remain to be determined. The coordination between axonal MTs and the spectrin/actin-based periodic membrane skeleton contributes to the neuronal shape dynamics and resistance to mechanical stress (Krieg et al., 2017). It is possible that gAnkB may play a role in maintaining the physical structural stability of the long and slender axons with extremely large aspect ratios by tethering cortical MTs to the membrane-attached actin cytoskeleton. It is of interest in this regard that the periodic membrane skeleton has recently been identified as a scaffold for receptor tyrosine kinase signaling (Zhou et al., 2019). Axonal branching is regulated by a variety of signals, including basic FGF, which potentially could modulate gAnkB–MT interactions in addition to its effects on Tau (Qiang et al., 2010). Recent studies also demonstrated that gAnkG can also couple with cortical MTs underneath plasma membranes and contribute to axon initial segment assembly (Fréal et al.,

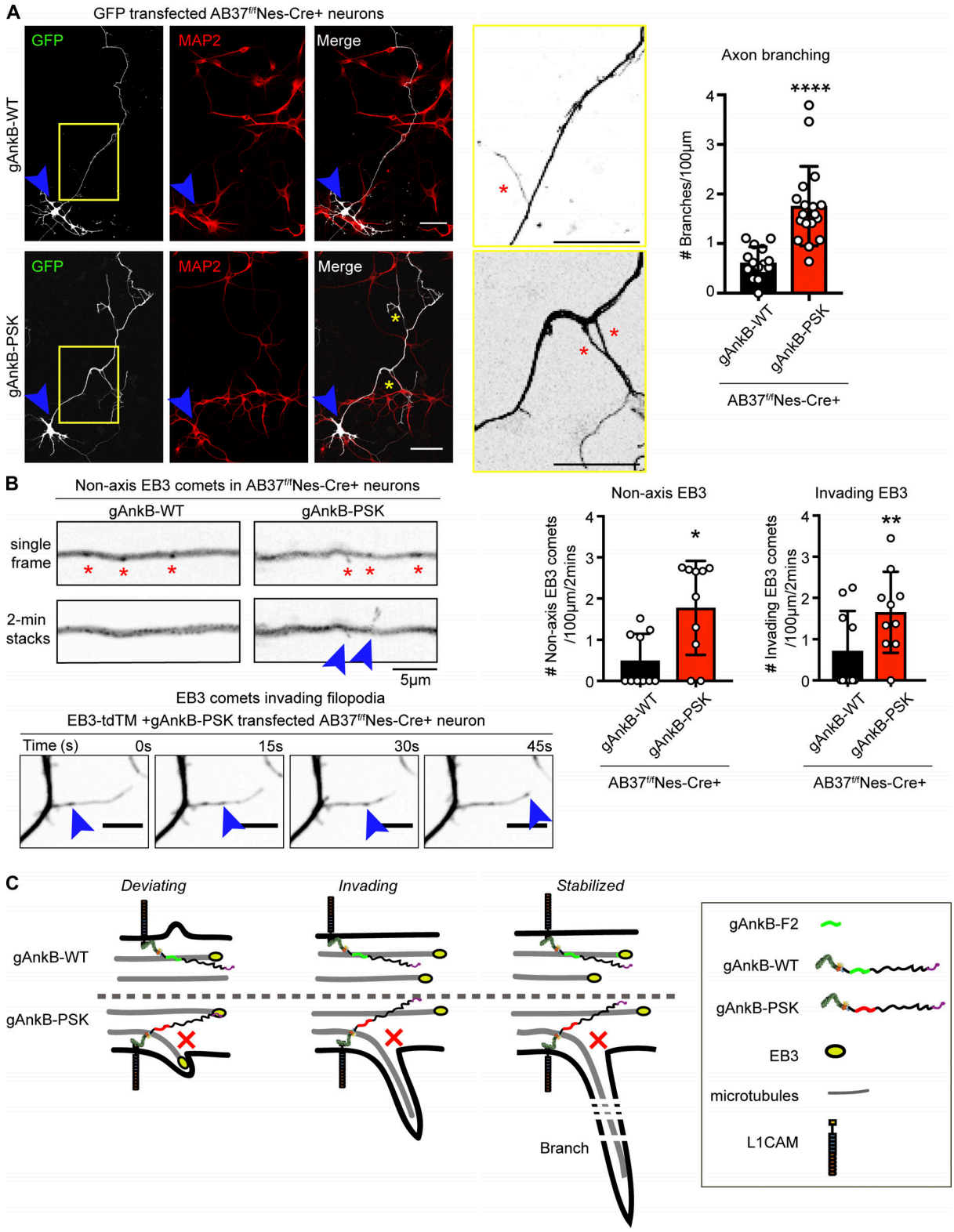

Figure 6. **The PSK mutant of gAnkB fails to suppress collateral axon branching. (A)** Fluorescence images of DIV4 cultured hippocampal neurons from *AB37$^{f/f}$ Nes-Cre^{+}* mice, which were transfected with GFP plus the full-length gAnkB cDNA (gAnkB-WT) or the cDNA-bearing MT-binding–deficient mutation (gAnkB-PSK). Blue arrowheads point to the cell body of the transfected neurons. A color-inverted high-magnification image of the yellow boxed region in the axon is displayed for better visualization of branches (marked with red asterisks; scale bars, 50 µm). Quantification of axon branching is displayed on the right (mean ± SEM; *t* test; ****P < 0.0001, *n* = 15 for gAnkB-WT or *n* = 18 for gAnkB-PSK, each from three batches of cultures). **(B)** Neurons from *AB37$^{f/f}$ Nes-Cre^{+}* mice were transfected with EB3-tdTM and gAnkB-WT (Video 5) or gAnkB-PSK (Video 6). Top: A time-lapse image from the axon is displayed as a single-frame or a 2-min stack image of transfected neurons (scale bar, 5 µm). Red asterisks indicate EB3 comets, and blue arrowheads indicate nonaxis EB3 comets. Bottom:

The steps of MT invading into a newly formed filopodium in the axon shaft of *AB37$^{f/f}$ Nes-Cre^{+}* neurons transfected with gAnkB-PSK mutant (Video 7; scale bar, 5 µm). Blue arrowhead tracks the movement of one EB3 comet. The number of nonaxis or invading EB3 was quantified and displayed on the right (mean ± SEM; *t* test; *P = 0.046 for nonaxis EB3; **P = 0.0063 for invading EB3; *n* = 10 cells in both conditions from three biological replicates). **(C)** Schematic diagrams demonstrating the process of axon-branching suppression by gAnkB-WT near the axonal membrane or failure of suppressing axon branching by gAnkB-PSK.

2019; Ichinose et al., 2019). Different from the direct coupling between gAnkB and MTs, gAnkG was found to associate with MTs via adaptor molecules (Ichinose et al., 2019), consistent with our finding showing that gAnkG only contains one 12-aa repeat sequence.

Interestingly, fruit flies also have evolved neuronal giant ankyrins with MT-binding activity in NSDs encoded by very large exons (Pielage et al., 2008; Stephan et al., 2015). However, *Drosophila melanogaster* and vertebrate giant ankyrins likely rose independently because their giant exons share minimal sequence homology and are located at different sites within their transcripts (Bennett and Walder, 2015; Koch et al., 2008; Pielage et al., 2008). *Drosophila* giant exons are located at the 3′ ends of transcripts, while vertebrate giant exons are located internally between the DD and spectrin-binding supramodule (Bennett and Lorenzo, 2016). In both cases, the giant exon-encoded sequence is enriched in predicted unstructured stretches, resulting in highly extended polypeptides. The similarities of axonal MT association and extended structures of independently evolved giant ankyrins in *Drosophila* and vertebrate neurons thus represent a striking example of convergent evolution.

The bipartite motif of gAnkB is conserved among eutherian and metatherian mammals, but not in monotreme mammals or other vertebrates, which retain a BG-box but lack the 15R module (Fig. S2 A). The last common ancestor of eutherian and metatherian mammals lived in the Jurassic period (dos Reis et al., 2012), suggesting that the mammalian bipartite motif has been preserved over 100 million years by positive selection. Interestingly, *AB37$^{f/f}$ Nes-Cre^{+}* mice lacking gAnkB in 90% of their central nervous system neurons survive with normal lifespan and normal learning but impaired social communication in selected areas (Yang et al., 2019). Mammalian gAnkB thus is not required for survival in a protected laboratory environment, but likely confers benefits in more complex settings and may operate at a social level.

Materials and methods

Cloning, expression, and protein purification

Full-length 440-kD ankyrin-B cDNA was based on a human annotated gAnkB (ENST00000264366.10). cDNA encoding human *ANK2* exon 37 plus flanking sequences used in this study was commercially synthesized (GENEWIZ) and inserted into the human 220-kD ankyrin-B cDNA using restriction enzyme digestion followed by ligation. The cDNA of gAnkB was then cloned into the multiple cloning site of a preconstructed vector under the β-actin promoter and a C-terminal Halo-tag sequence (gift from Dr. Gary Banker, Oregon Health and Science University, Portland, OR). A cDNA fragment encoding the MT-binding mutant (the PSK mutant) of gAnkB repeats was synthesized and used to replace the corresponding sequence in the full-length gAnkB cDNA by using the In-Fusion Cloning Kit (Takara Bio). The mutations were confirmed by Sanger sequencing. EB3-tdTM was a gift from Dr. Erik Dent (plasmid 50708; Addgene). pCAG-GFP was a gift from Dr. Gary Banker.

All of the ankyrin fragment coding sequences were PCR amplified from the full-length human 440-kD AnkB or rat 480-kD AnkG cDNA harboring plasmids. Tau coding sequence was PCR amplified from a human Tau full-length template (a gift from Dr. Robert Qi, Hong Kong University of Science and Technology, Hong Kong). Each of the coding sequences was inserted into a modified PET32a vector, which could express Trx-His$_6$-tagged or Trx-3xStrepII-His$_6$ tagged fusion proteins in *E. coli*.

The N-terminal Trx-His$_6$-tagged or Trx-3xStrepII-His$_6$-tagged proteins were expressed in *E. coli* BL21 (DE3) and purified using the methods described previously (Chen et al., 2017). In brief, 200-ng plasmids were transformed into 50-µl *E. coli* BL21 (DE3) competent cells. On the second day, the cells were inoculated to 1–2-liter Lysogeny broth medium and incubated at 37°C with shaking at 200 rpm. When UV absorbance at 600 nm of the cultured cells reached 0.8, the cells were induced by adding 0.15 mM IPTG, and the culture was shifted to 16°C for 20 h with shaking at 200 rpm. The cells were then pelleted by centrifugation at 3,000 *g* for 15 min, resuspended with 40 ml resuspension buffer (50 mM Tris, 500 mM NaCl, and 5 mM imidazole, pH 8.0), and lysed by a high-pressure homogenizer machine at 4°C, followed by high-speed centrifugation at 39,000 *g* for 20 min. The supernatant was injected into a Ni^{2+}-NTA agarose affinity column (containing 5 ml of Ni^{2+} Sepharose 6 Fast Flow beads, 17531803; GE Healthcare). The column was incubated for 15 min and washed twice with 30 ml washing buffer (50 mM Tris, 500 mM NaCl, and 15 mM imidazole, pH 8.0). Then the proteins on the column were eluted with 15 ml elution buffer (50 mM Tris, 500 mM NaCl, and 1 M imidazole, pH 8.0). The eluted proteins were applied to a size exclusion column (HiLoad 26/600 Superdex 200 pg column; GE Healthcare) with buffer containing 50 mM Tris-HCl, 1 mM DTT, and 1 mM EDTA, pH 7.8, with 100 mM NaCl. The fused Trx-His$_6$ tag was cleaved by incubating each recombinant protein with HRV 3C protease overnight at 4°C. The cleaved tag of each protein was removed by another step of the size exclusion chromatography.

All of the unlabeled and rhodamine/Hylate-488–labeled tubulin heterodimer proteins were purchased from Cytoskeleton Inc. (TL590M, TL488M, and T240). These commercially purchased tubulins were purified from porcine brain tissue in >99% purity and supplied as lyophilized powders.

Fluorescence labeling of recombinant proteins

Purified recombinant proteins (at concentrations of 5–10 mg/ml) were incubated with fluorescent dye (Alexa Fluor 488 NHS Ester, A20100, Thermo Fisher Scientific; Cyanine3 NHS Ester,

21020, Lumiprobe Corporation) with a stoichiometric ratio of 1:1 to 1:2 (protein/dye) in 100 mM $NaHCO_3$, pH 8.3, 50 mM NaCl, and 1 mM DTT buffer at room temperature and protected from light for 1 h, followed by a step of gel filtration chromatography to remove unconjugated dye molecules and to exchange proteins into PEM buffer (80 mM Pipes, 1 mM EGTA, and 1 mM $MgCl_2$, pH 6.8) or reaction buffer (10 mM Hepes, 50 mM KCl, 1 mM DTT, and 20 µM Taxol, pH 7.7).

Taxol-induced tubulin polymerization in vitro

Lyophilized tubulin powders were dissolved by using PEM buffer (80 mM Pipes, 1 mM EGTA, and 1 mM $MgCl_2$, pH 6.8) and incubated on ice for 5 min to make a 20-mg/ml tubulin stock solution. This stock solution was then diluted to a 2-mg/ml tubulin solution with PEM buffer supplemented with 1 mM GTP (Sigma-Aldrich) and 1 mM DTT (Sigma-Aldrich) to make a polymerization mixture. This mixture was subjected to 150,000 *g* centrifugation for 5 min at 4°C to remove small amounts of tubulin aggregates and then incubated at 37°C for 1 h. Taxol (paclitaxel, T7191, lot no. MKCH9403; Sigma-Aldrich) was then added in stepwise fashion to the polymerization mixture from low concentration (2 µM) to high concentration (200 µM) to induce the polymerization of tubulins. Between each step of Taxol addition, the polymerization mixture was incubated at 37°C for 10 min without shaking.

MT cosedimentation assay

A 50-µl aliquot of the above-mentioned polymerized MTs was mixed with 100 µl of each recombinant protein at 5 µM or 10 µM (Trx protein at 15 or 30 µM) in reaction buffer. The recombinant proteins were centrifuged at 150,000 *g* for 5 min to remove potential aggregates before use. Each mixture was incubated at room temperature for 15 min before being gently added to a centrifuge tube, which was prefilled with 150 µl sucrose cushion solution (40% wt/vol sucrose, 10 mM Hepes, 50 mM KCl, and 20 µM Taxol, pH 7.7). The mixture was then centrifuged at 150,000 *g* for 20 min at 25°C. Supernatant (100 µl was withdrawn, and the rest was discarded) and pellet fractions (washed two times with the reaction buffer) were collected and mixed with 100 µl SDS-PAGE loading buffer (125 mM Tris-HCl, pH 6.8, 10% SDS, 20% glycerol, and 10% β-mercaptoethanol). The samples were then boiled at 90°C to dissolve the pellets and analyzed by SDS-PAGE followed by Coomassie blue staining. Stained gels were imaged by using the ChemiDoc Touch Imaging System (Bio-Rad Laboratories) and processed by using Bio-Rad Image Lab software. Quantification of the bands was done by using ImageJ software. The amount of proteins in the supernatant and pellet fractions were back-calculated on the basis of the protein band intensity quantification result and the input sample concentration and loading ratio.

Imaging-based in vitro MT-bundling assay

A 10-µl aliquot of Taxol-stabilized MTs was mixed with 20 µl testing proteins (contains ∼30% fluorescence-labeled proteins) at 5 µM or 15 µM. Each mixture was then diluted 50 times with reaction buffer (10 mM Hepes, 50 mM KCl, 1 mM DTT, and 20 µM Taxol, pH 7.7), sealed in a glass coverslip, and imaged immediately at room temperature under a Zeiss LSM880 inverted confocal microscope with 40× or 63× NA 1.4 oil objective lens. Z-stack images were acquired by using ZEN software with the following settings: 1,024 × 1,024 or 2,048 × 2,048 pixels, four-line averaging, 0.24-µs pixel dwell speed, and 1 airy unit pinhole. The images were then processed by maximum intensity projection. The brightness of the images in Fig. 2 C, Fig. 4 B, and Fig. 5 B was adjusted for better visualization of the unbundled single-MT filaments. MT filament or bundle widths in the fluorescence images are quantified as follows. For the unbundled MTs (e.g., the GFP control group in Fig. 2 C or the 5R group in Fig. 4 B), the MTs were quite homogeneous, and the widths of these MTs were measured using ImageJ software by randomly choosing sufficient numbers of MTs. For the bundled MTs, if the bundled MT filaments were not branched (e.g., the thick filaments in the 10R and 15R groups in Fig. 4 B), their widths were simply defined by measuring the distances between two edges in the middle part of each thick filament. If the bundled filaments contained multiple strands (e.g., the gAnkB-F2 group in Fig. 2 C), we measured the width of the high-order bundling sites, defined as the regions where branching strands were tightly packed with each other and the gap between two thinner strands was narrower than 1 µm.

Circular dichroism

The circular dichroism spectrum of the Trx-tag–removed gAnkB-F2 was measured on a Chirascan spectropolarimeter (Applied Photophysics) using a cell path length of 1 mm at a temperature range from 18°C to 84°C with a 2°C interval. Each spectrum was collected with three scans spanning a spectral window of 195–260 nm. The samples were dissolved in 25 mM Tris buffer containing 50 mM NaCl, 0.5 mM EDTA, and 0.5 mM DTT at pH 7.5. The protein concentration used in the circular dichroism experiment was 20 µM.

EM

Negative stain analysis was performed using 300-mesh carbon-coated copper grids (EMResolutions). Grids were glow discharged for 30 s at 40 mA using a GloQube glow discharger (Quorum Technologies). A 5-µl drop of 1:8 dilution sample was applied onto the grid and incubated for 2 min. The sample was then quickly blotted away, and a 5-µl drop of 2% uranyl acetate solution was applied for 30 s before blotting to complete dryness. Negative stain images were collected using a Talos L120C transmission electron microscope (Thermo Fisher Scientific) operating at 120 kV. Images were recorded using a 4k × 4k BM-Ceta camera (Thermo Fisher Scientific) at a nominal magnification of 22,000× (6.43 Å/pixel at the specimen level).

gAnkB-specific antibody

The rabbit anti-gAnkB antibody was generated in house. Five peptides (10 mg each) with addition of N-terminal lysine residues to facilitate Schiff base chemistry from gAnkB residues 1443–1620 were synthesized (Thermo Fisher Scientific). The sequences for these polypeptides were as follows: KSHLVNEVPV-LASPDLLSE, KAAEEEPGEPFEIVERV, KVNEILRSGTCTRDESS, EEEW-VIVSDEEIEEARQK, and GLVNYLTDDLNTCVPLPK. The peptides were

dissolved in 50 mM sodium phosphate buffer (pH 7.4) to 10 mg/ml, mixed, and coupled overnight with glutaraldehyde-activated rabbit serum albumin (RSA; Sigma-Aldrich; 5 mg/ml RSA reacted 60 min/24°C with glutaraldehyde [EM grade, 1% final; Sigma-Aldrich], followed by overnight dialysis to remove free glutaraldehyde). Peptide–RSA conjugates were mixed at a 1:1 ratio with Freund's complete (first immunization) or Freund's incomplete (subsequent immunizations; Sigma-Aldrich) adjuvant, and each time, a 0.5-ml mixture was injected subcutaneously at multiple sites in each New Zealand white rabbit (aged 3–4 mo). All rabbit procedures were performed following the guidelines of the Duke Division of Laboratory Animal Resources. The final pooled sera after five injections were from three rabbits that reacted specifically with a 440-kD polypeptide in WT but not in *AB37*$^{f/f}$ *Nes-Cre*$^{+}$ mice brain lysates. Sera were diluted 1:1 with 150 mM NaCl, 10 mM Na_3PO_4, 1 mM EDTA, 1 mM NaN_3, and 0.2% Triton X-100 and heat inactivated at 56°C for 15 min. A quantity of 70 ml of pooled sera was preadsorbed with RSA-Sepharose and then adsorbed to the mixed peptides coupled to Sepharose (5 ml of Sepharose). The column was then washed first with 500 mM NaCl, 10 mM sodium phosphate buffer, and 0.1% Triton X-100 (10× column volumes); followed by 2 M urea, 0.1 M glycine, and 0.1% Triton X-100 (2× column volumes); and finally with 150 mM NaCl, 10 mM sodium phosphate, 1 mM EDTA, and 1 mM NaN_3 until A_{280} was below 0.01. Finally, antibodies were eluted with 4 M $MgCl_2$ and dialyzed into antibody storage buffer (150 mM NaCl, 10 mM sodium phosphate buffer, 1 mM EDTA, 1 mM NaN_3, and 50% glycerol, vol/vol). The specificity of purified final antibody was tested in immunoblots, cell staining, and brain paraffin section staining of brain tissue from the WT mice with *AB37*$^{f/f}$ *Nes-Cre*$^{+}$ mice as a negative control. The Ig concentration for paraffin brain sections and cultured hippocampal neurons was 1 µg/ml.

In-gel Western blotting for detecting gAnkB

Mouse brain tissue or HEK293T cells were collected and homogenized for 30 s in 9 vol/wt 65°C prewarmed homogenization buffer (8 M urea, 5% SDS [wt/vol], 50 mM Tris, pH 7.4, 5 mM EDTA, 5 mM N-ethylmelanamide, protease and phosphatase inhibitors) and heated at 65°C for 15 min until the homogenate was cleared. The homogenate was mixed with 5× PAGE buffer (5% SDS [wt/vol], 25% sucrose [wt/vol], 50 mM Tris, pH 8, 5 mM EDTA, and bromophenol blue) and heated for 15 min at 65°C. Samples were run on a 3.5–17.5% 0.75-mm gradient gel in Fairbanks running buffer (40 mM Tris, pH 7.4, 20 mM NaAc, 2 mM EDTA, and 0.2% SDS [wt/vol]). Gels for in-gel Western blots were immediately fixed in 50% isopropanol plus 7% glacial acetic acid for 15 min and washed two times for 10 min with deionized water.

Gels were incubated with primary antibodies (rabbit anti–total ankyrin-B, 1:2,000 dilution) in 5% BSA (wt/vol) in TBS overnight at 4°C on a shaker. After two washes with TBST (TBS with 0.05% vol/vol Tween 20), gels were incubated with secondary antibodies (goat antirabbit 800CW, 1:10,000 dilution; 926-32211, LI-COR Biosciences) for 2 h at room temperature on a shaker. Gels were extensively washed with TBST for 1 h each with two final washes in TBS (10 min each). Gels were imaged on the LI-COR Odyssey at 0.37-mm custom offset.

Hippocampal neuron culture, transfection, and immunostaining

Primary hippocampal neurons and astrocytes were prepared as described previously (Kaech and Banker, 2006; Kaech et al., 2012). Briefly, hippocampi were dissected from genotyped postnatal 0–1-d mice, trypsinized, dissociated, and plated onto poly-L-lysine–coated 18-mm glass coverslips in preconditioned glia feeder dishes (~200,000 neurons/60-mm culture dish). Cultures were grown in Neurobasal-A medium plus B27 supplement (2%) and GlutaMAX (1%; Thermo Fisher Scientific) and maintained at 37°C in an incubator with 5% CO_2.

Constructs were transfected into 3-d-old hippocampal neurons or astrocytes with Lipofectamine 2000 (13778075; Thermo Fisher Scientific) and subsequently fixed with 4% (wt/vol) PFA with 4% (wt/vol) sucrose in PBS for 15 min at 37°C before antibody staining. Fixed neurons were washed with PBS, permeabilized with 0.25% Triton X-100 for 5 min, and then blocked with 5% BSA in PBS for 1 h. The chicken anti-MAP2 (1:1,000) antibody from Abcam (AB5392) was diluted in blocking buffer (5% BSA in PBS, wt/vol) and incubated at 4°C overnight. The next day, the neurons were washed with PBS, then incubated with the Alexa Fluor 594–conjugated secondary antibodies (1:500; Thermo Fisher Scientific) in blocking buffer for 1 h at room temperature. Finally, the fixed neurons were mounted with Prolong Diamond (Thermo Fisher Scientific) onto glass slides and allowed to cure for a minimum of 24 h at room temperature before imaging by confocal microscopy (Zeiss LSM780 inverted confocal microscope). Astrocytes expressing constructs with a HaloTag were treated with 50 nM Janelia Farm 549 dye (Grimm et al., 2015) for 10 min and washed for 10 min before fixation or imaging.

Astrocyte culture, fixation, and staining for MT visualization

Mouse cortices were dissected from postnatal day 1 mice, trypsinized, dissociated, and plated in MEM (Thermo Fisher Scientific) supplemented with 0.6% glucose (wt/vol; G8769; Sigma-Aldrich), penicillin (100 U/ml), streptomycin (100 mg/ml), and 10% (vol/vol) horse serum (Thermo Fisher Scientific). Media were changed after 1 d and continued to be changed every 2–3 d until cell density reached 40–50% confluence for transfection. Cells were transfected with Lipofectamine 2000 (Thermo Fisher Scientific) and fixed by a modified protocol to visualize the cytoskeleton (Smith, 1994). Briefly, cells were fixed in prewarmed (37°C) PHEM buffer (60 mM Pipes, 25 mM Hepes, 10 mM EGTA, 2 mM $MgCl_2$, 3.7% [wt/vol] PFA/sucrose, 0.25% [wt/vol] glutaraldehyde, and 0.1% [vol/vol] Triton X-100) for 15 min at room temperature. The fixed cells were sequentially washed three or four times with 1× PBS, quenched with 50 mM NH_4Cl/PBS for ~10 min, blocked with 5% (wt/vol) BSA at room temperature for 1 h, and finally incubated with anti-tubulin antibody (1:1,000; 53-4502-80; eBioscience) or AnkB antibody (1:1,000) at 4°C overnight. The next day, cells were washed with 1× PBS three times, incubated with Alexa Fluor 594 or Alexa Fluor 488 secondary antibodies for 1 h at room temperature, and washed with 1× PBS three times again before being mounted for imaging. Images were acquired on an LSM780 inverted confocal microscope with a 63×/NA 1.4 oil lens objective (Zeiss).

Live-cell imaging of EB3 comets and quantification

Cultured hippocampal neurons were transfected with EB3-tdTM plasmids at DIV3 with Lipofectamine 2000 (13778075; Thermo Fisher Scientific). On DIV4, neurons were imaged on an Andor XD revolution spinning disk confocal microscope (Oxford Instruments; spinning-disk confocal head, Yokogawa CSU-X1, 5,000 rpm) equipped with an electron multiplying charge-coupled device camera. Neurons were changed to prewarmed live-cell imaging solution (A14291DJ; Thermo Fisher Scientific) to reduce background. The whole imaging stage and objectives were maintained at 37°C and 5% CO_2 in an enclosure. A 100×/NA 1.4 oil U PlanSApo DIC objective (Olympus) was used to acquire image streams of 40 frames (3 s per frame; exposure time, 200 ms; 30% laser power). For the EB3 stacking images, a series of images from 40 time points were stacked together using the Z-projection macro in Fiji software. The signal of the stacked images was inverted to best display the trajectory of EB3 comets. The numbers of nonaxis EB3 were quantified by looking at the EB3 comets that were initiated from the axon shaft, then moved off the major axon shaft in a 2-min video. The invading EB3 comets were quantified by looking at EB3 comets that were invading into a preexistent filopodia in a 2-min video. The number of EB3 comets was normalized to the length of axons.

General statistical analyses

Statistical analyses and graph generation were performed using Prism 7 software (GraphPad Software). The data are presented as mean ± SEM. The Shapiro-Wilk test for normality was used to test whether data assumed a gaussian distribution. An unpaired, two-tailed Student's *t* test was used when comparing two groups with a normal distribution, and the Mann-Whitney *U* test was used when comparing two groups without a normal distribution. $P < 0.05$ was considered significant. The statistical methods, sample volumes, and P values are stated in each figure legend.

Online supplemental material

Fig. S1 shows the gene editing schematic of *AB37$^{f/f}$ Nes-Cre* mice and an immunoblot of brain AnkB. It also shows an EB3 comet that did not invade into a filopodium in the axon of an AB37$^{f/f}$ Nes-Cre^{-} neuron. Fig. S2 shows the sequence alignment and sequence logo plot of the gAnkB 15 repeats from different species. Fig. S3 shows the evidence that the gAnkB-F2 protein sequence is intrinsically disordered. It also shows the gap width between bundled MTs measured from EM images. Fig. S4 shows that the negative control, gAnkB-CD, cannot bind to MTs. It also shows that gAnkG possesses MT-binding activity. Fig. S5 shows that replacements of Asp/Glu-Lys/Arg at the end of each 12-aa repeat with Ala-Gly do not affect the MT binding of gAnkB 15 repeats. Video 1 displays nonaxis EB3 comets in a WT axon. Video 2 shows nonaxis EB3 comets in gAnkB-knockout axon. In Video 3, an invading EB3 is seen in gAnkB-knockout filopodia. Video 4 exhibits an invading EB3 comet in WT filopodia. Video 5 displays gAnkB-WT rescue nonaxis EB3 comets. Video 6 shows gAnkB-PSK rescue nonaxis EB3 comets. In Video 7, using gAnkB-PSK to rescue invading EB3 comets in filopodia is shown.

Acknowledgments

We thank Dr. Vann Bennett for advice, support, and discussions throughout the course of the study. We thank Danwei Wu for analyzing the expression level of ankyrin-B in *AB37$^{f/f}$ Nes-Cre* mice. M. Zhang is a Kerry Holdings Professor in Science and a Senior Fellow of Institute for Advanced Study at Hong Kong University of Science and Technology.

This work was supported by Research Grants Council of Hong Kong, University Grants Committee grants 16100517, C6004-17G, and AoE-M09-12 (M. Zhang).

The authors declare no competing financial interests.

Author contributions: K. Chen and R. Yang conceived the project, designed the experiments, analyzed the data, drafted the article, and contributed unpublished essential data or reagents. Y. Li performed the biochemical experiments, analyzed the data, helped with revising the manuscript, and contributed unpublished essential data or reagents. J.C. Zhou acquired the EM images and analyzed and interpreted the data. M. Zhang conceived the project, designed the experiments, analyzed the data, wrote the manuscript, and coordinated the research.

Submitted: 10 October 2019
Revised: 18 February 2020
Accepted: 27 April 2020

References

Akhmanova, A., and M.O. Steinmetz. 2008. Tracking the ends: a dynamic protein network controls the fate of microtubule tips. *Nat. Rev. Mol. Cell Biol.* 9:309–322. https://doi.org/10.1038/nrm2369

Armijo-Weingart, L., and G. Gallo. 2017. It takes a village to raise a branch: Cellular mechanisms of the initiation of axon collateral branches. *Mol. Cell. Neurosci.* 84:36–47. https://doi.org/10.1016/j.mcn.2017.03.007

Bennett, V., and D.N. Lorenzo. 2016. An adaptable spectrin/ankyrin-based mechanism for long-range organization of plasma membranes in vertebrate tissues. *In Dynamic plasma membranes: Portals between cells and physiology*. Current Topics in Membranes. Vol. 77. V. Bennett, editor. Academic Press, Cambridge, MA. 143–184. https://doi.org/10.1016/bs.ctm.2015.10.001

Bennett, V., and K. Walder. 2015. Evolution in action: giant ankyrins awake. *Dev. Cell.* 33:1–2. https://doi.org/10.1016/j.devcel.2015.03.017

Bouquet, C., S. Soares, Y. von Boxberg, M. Ravaille-Veron, F. Propst, and F. Nothias. 2004. Microtubule-associated protein 1B controls directionality of growth cone migration and axonal branching in regeneration of adult dorsal root ganglia neurons. *J. Neurosci.* 24:7204–7213. https://doi.org/10.1523/JNEUROSCI.2254-04.2004

Chan, W., E. Kordeli, and V. Bennett. 1993. 440-kD ankyrinB: structure of the major developmentally regulated domain and selective localization in unmyelinated axons. *J. Cell Biol.* 123:1463–1473. https://doi.org/10.1083/jcb.123.6.1463

Chen, K., J. Li, C. Wang, Z. Wei, and M. Zhang. 2017. Autoinhibition of ankyrin-B/G membrane target bindings by intrinsically disordered segments from the tail regions. *eLife*. 6. e29150. https://doi.org/10.7554/eLife.29150

Davis, J.Q., and V. Bennett. 1984. Brain ankyrin. A membrane-associated protein with binding sites for spectrin, tubulin, and the cytoplasmic domain of the erythrocyte anion channel. *J. Biol. Chem.* 259:13550–13559.

Davis, L.H., E. Otto, and V. Bennett. 1991. Specific 33-residue repeat(s) of erythrocyte ankyrin associate with the anion exchanger. *J. Biol. Chem.* 266:11163–11169.

Dehmelt, L., and S. Halpain. 2005. The MAP2/Tau family of microtubule-associated proteins. *Genome Biol.* 6:204. https://doi.org/10.1186/gb-2004-6-1-204

Dent, E.W., J.L. Callaway, G. Szebenyi, P.W. Baas, and K. Kalil. 1999. Reorganization and movement of microtubules in axonal growth cones and

developing interstitial branches. *J. Neurosci.* 19:8894–8908. https://doi.org/10.1523/JNEUROSCI.19-20-08894.1999

De Rubeis, S., X. He, A.P. Goldberg, C.S. Poultney, K. Samocha, A.E. Cicek, Y. Kou, L. Liu, M. Fromer, S. Walker, et al; UK10K Consortium. 2014. Synaptic, transcriptional and chromatin genes disrupted in autism. *Nature.* 515:209–215. https://doi.org/10.1038/nature13772

dos Reis, M., J. Inoue, M. Hasegawa, R.J. Asher, P.C.J. Donoghue, and Z. Yang. 2012. Phylogenomic datasets provide both precision and accuracy in estimating the timescale of placental mammal phylogeny. *Proc. Biol. Sci.* 279:3491–3500. https://doi.org/10.1098/rspb.2012.0683

Fache, V., J. Gaillard, D. Van Damme, D. Geelen, E. Neumann, V. Stoppin-Mellet, and M. Vantard. 2010. *Arabidopsis* kinetochore fiber-associated MAP65-4 cross-links microtubules and promotes microtubule bundle elongation. *Plant Cell.* 22:3804–3815. https://doi.org/10.1105/tpc.110.080606

Fréal, A., D. Rai, R.P. Tas, X. Pan, E.A. Katrukha, D. van de Willige, R. Stucchi, A. Aher, C. Yang, A.F.M. Altelaar, et al. 2019. Feedback-driven assembly of the axon initial segment. *Neuron.* 104:305–321.e8. https://doi.org/10.1016/j.neuron.2019.07.029

Gaillard, J., E. Neumann, D. Van Damme, V. Stoppin-Mellet, C. Ebel, E. Barbier, D. Geelen, and M. Vantard. 2008. Two microtubule-associated proteins of *Arabidopsis* MAP65s promote antiparallel microtubule bundling. *Mol. Biol. Cell.* 19:4534–4544. https://doi.org/10.1091/mbc.e08-04-0341

Gaillard, J., V. Ramabhadran, E. Neumanne, P. Gurel, L. Blanchoin, M. Vantard, and H.N. Higgs. 2011. Differential interactions of the formins INF2, mDia1, and mDia2 with microtubules. *Mol. Biol. Cell.* 22:4575–4587. https://doi.org/10.1091/mbc.e11-07-0616

Grimm, J.B., B.P. English, J. Chen, J.P. Slaughter, Z. Zhang, A. Revyakin, R. Patel, J.J. Macklin, D. Normanno, R.H. Singer, et al. 2015. A general method to improve fluorophores for live-cell and single-molecule microscopy. *Nat. Methods.* 12:244–250: 3: 250. https://doi.org/10.1038/nmeth.3256

Homma, N., Y. Takei, Y. Tanaka, T. Nakata, S. Terada, M. Kikkawa, Y. Noda, and N. Hirokawa. 2003. Kinesin superfamily protein 2A (KIF2A) functions in suppression of collateral branch extension. *Cell.* 114:229–239. https://doi.org/10.1016/S0092-8674(03)00522-1

Ichinose, S., T. Ogawa, X. Jiang, and N. Hirokawa. 2019. The spatiotemporal construction of the axon initial segment via KIF3/KAP3/TRIM46 transport under MARK2 signaling. *Cell Rep.* 28:2413–2426.e7. https://doi.org/10.1016/j.celrep.2019.07.093

Iossifov, I., B.J. O'Roak, S.J. Sanders, M. Ronemus, N. Krumm, D. Levy, H.A. Stessman, K.T. Witherspoon, L. Vives, K.E. Patterson, et al. 2014. The contribution of de novo coding mutations to autism spectrum disorder. *Nature.* 515:216–221. https://doi.org/10.1038/nature13908

Kaech, S., and G. Banker. 2006. Culturing hippocampal neurons. *Nat. Protoc.* 1:2406–2415. https://doi.org/10.1038/nprot.2006.356

Kaech, S., C.-F. Huang, and G. Banker. 2012. Short-term high-resolution imaging of developing hippocampal neurons in culture. *Cold Spring Harb. Protoc.* 2012:340–343. https://doi.org/10.1101/pdb.prot068247

Kalil, K., and E.W. Dent. 2014. Branch management: mechanisms of axon branching in the developing vertebrate CNS. *Nat. Rev. Neurosci.* 15:7–18. https://doi.org/10.1038/nrn3650

Kellogg, E.H., N.M.A. Hejab, S. Poepsel, K.H. Downing, F. DiMaio, and E. Nogales. 2018. Near-atomic model of microtubule-tau interactions. *Science.* 360:1242–1246. https://doi.org/10.1126/science.aat1780

Kleele, T., P. Marinković, P.R. Williams, S. Stern, E.E. Weigand, P. Engerer, R. Naumann, J. Hartmann, R.M. Karl, F. Bradke, et al. 2014. An assay to image neuronal microtubule dynamics in mice. *Nat. Commun.* 5:4827. https://doi.org/10.1038/ncomms5827

Koch, I., H. Schwarz, D. Beuchle, B. Goellner, M. Langegger, and H. Aberle. 2008. *Drosophila* ankyrin 2 is required for synaptic stability. *Neuron.* 58:210–222. https://doi.org/10.1016/j.neuron.2008.03.019

Krieg, M., J. Stühmer, J.G. Cueva, R. Fetter, K. Spilker, D. Cremers, K. Shen, A.R. Dunn, and M.B. Goodman. 2017. Genetic defects in β-spectrin and tau sensitize *C. elegans* axons to movement-induced damage via torque-tension coupling. *eLife.* 6. e20172. https://doi.org/10.7554/eLife.20172

Kunimoto, M., E. Otto, and V. Bennett. 1991. A new 440-kD isoform is the major ankyrin in neonatal rat brain. *J. Cell Biol.* 115:1319–1331. https://doi.org/10.1083/jcb.115.5.1319

Leterrier, C., J. Potier, G. Caillol, C. Debarnot, F. Rueda Boroni, and B. Dargent. 2015. Nanoscale architecture of the axon initial segment reveals an organized and robust scaffold. *Cell Rep.* 13:2781–2793. https://doi.org/10.1016/j.celrep.2015.11.051

Lorenzo, D.N., A. Badea, J. Davis, J. Hostettler, J. He, G. Zhong, X. Zhuang, and V. Bennett. 2014. A PIK3C3-ankyrin-B-dynactin pathway promotes axonal growth and multiorganelle transport. *J. Cell Biol.* 207:735–752. https://doi.org/10.1083/jcb.201407063

Menon, S., and S. Gupton. 2018. Recent advances in branching mechanisms underlying neuronal morphogenesis. *F1000 Res.* 7:1779. https://doi.org/10.12688/f1000research.16038.1

Otto, E., M. Kunimoto, T. McLaughlin, and V. Bennett. 1991. Isolation and characterization of cDNAs encoding human brain ankyrins reveal a family of alternatively spliced genes. *J. Cell Biol.* 114:241–253. https://doi.org/10.1083/jcb.114.2.241

Pielage, J., L. Cheng, R.D. Fetter, P.M. Carlton, J.W. Sedat, and G.W. Davis. 2008. A presynaptic giant ankyrin stabilizes the NMJ through regulation of presynaptic microtubules and transsynaptic cell adhesion. *Neuron.* 58:195–209. https://doi.org/10.1016/j.neuron.2008.02.017

Qiang, L., W. Yu, A. Andreadis, M. Luo, and P.W. Baas. 2006. Tau protects microtubules in the axon from severing by katanin. *J. Neurosci.* 26:3120–3129. https://doi.org/10.1523/JNEUROSCI.5392-05.2006

Qiang, L., W. Yu, M. Liu, J.M. Solowska, and P.W. Baas. 2010. Basic fibroblast growth factor elicits formation of interstitial axonal branches via enhanced severing of microtubules. *Mol. Biol. Cell.* 21:334–344. https://doi.org/10.1091/mbc.e09-09-0834

Scott, C.W., A.B. Klika, M.M.S. Lo, T.E. Norris, and C.B. Caputo. 1992. Tau protein induces bundling of microtubules in vitro: comparison of different tau isoforms and a tau protein fragment. *J. Neurosci. Res.* 33:19–29. https://doi.org/10.1002/jnr.490330104

Smith, C.L.. 1994. Cytoskeletal movements and substrate interactions during initiation of neurite outgrowth by sympathetic neurons in vitro. *J. Neurosci.* 14:384–398. https://doi.org/10.1523/JNEUROSCI.14-01-00384.1994

Stephan, R., B. Goellner, E. Moreno, C.A. Frank, T. Hugenschmidt, C. Genoud, H. Aberle, and J. Pielage. 2015. Hierarchical microtubule organization controls axon caliber and transport and determines synaptic structure and stability. *Dev. Cell.* 33:5–21. https://doi.org/10.1016/j.devcel.2015.02.003

Tortosa, E., L.C. Kapitein, and C.C. Hoogenraad. 2016. Microtubule Organization and Microtubule-Associated Proteins (MAPs). *In* Dendrites: Development and Disease. K. Emoto, R.O. Wong, E. Huang, and C.C. Hoogenraad, editors. Springer Japan, Tokyo. pp. 31–75. https://doi.org/10.1007/978-4-431-56050-0_3

Tymanskyj, S.R., B. Yang, A. Falnikar, A.C. Lepore, and L. Ma. 2017. MAP7 regulates axon collateral branch development in dorsal root ganglion neurons. *J. Neurosci.* 37:1648–1661. https://doi.org/10.1523/JNEUROSCI.3260-16.2017

Xu, K., G. Zhong, and X. Zhuang. 2013. Actin, spectrin, and associated proteins form a periodic cytoskeletal structure in axons. *Science.* 339:452–456. https://doi.org/10.1126/science.1232251

Yang, R., K.K. Walder-Christensen, N. Kim, D. Wu, D.N. Lorenzo, A. Badea, Y.-H. Jiang, H.H. Yin, W.C. Wetsel, and V. Bennett. 2019. *ANK2* autism mutation targeting giant ankyrin-B promotes axon branching and ectopic connectivity. *Proc. Natl. Acad. Sci. USA.* 116:15262–15271. https://doi.org/10.1073/pnas.1904348116

Yu, W., F.J. Ahmad, and P.W. Baas. 1994. Microtubule fragmentation and partitioning in the axon during collateral branch formation. *J. Neurosci.* 14:5872–5884. https://doi.org/10.1523/JNEUROSCI.14-10-05872.1994

Zhong, G., J. He, R. Zhou, D. Lorenzo, H.P. Babcock, V. Bennett, and X. Zhuang. 2014. Developmental mechanism of the periodic membrane skeleton in axons. *eLife.* 3. e04581. https://doi.org/10.7554/eLife.04581

Zhou, R., B. Han, C. Xia, and X. Zhuang. 2019. Membrane-associated periodic skeleton is a signaling platform for RTK transactivation in neurons. *Science.* 365:929–934. https://doi.org/10.1126/science.aaw5937

Supplemental material

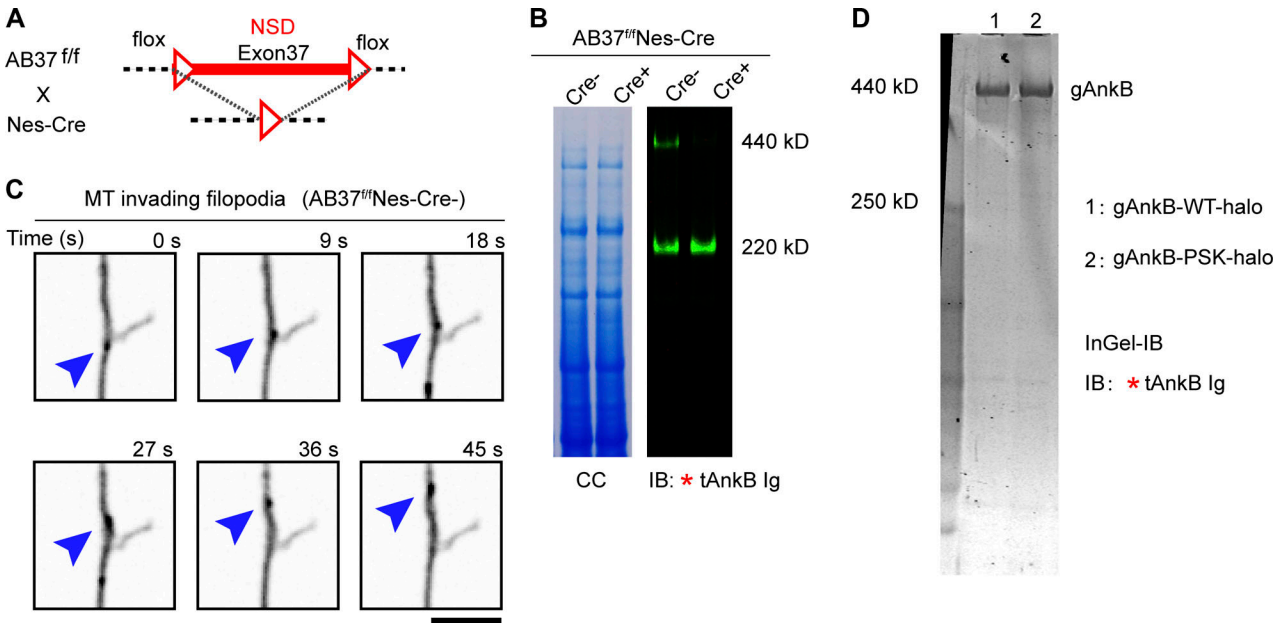

Figure S1. **Specific knockout of giant AnkB isoform in mouse neurons. (A)** Schematic of the gene editing of *AB37$^{f/f}$ Nes-Cre* mice. Triangles indicate the flox sites. The red line indicates the coding sequence of exon 37 for the gAnkB NSD. **(B)** In-gel Western blotting of brain lysate blotted with tAnkB antibody (right lane; IB). A repeated loading gel is stained with Coomassie blue as a loading control (left lane; CC). **(C)** Time-series images show an EB3 comet that did not invade into a filopodium in the axon of an *AB37$^{f/f}$ Nes-Cre^{-}* neuron (Video 4; scale bar, 5 µm). Blue arrowhead tracks the movement of one EB3 comet. **(D)** In-gel Western blot analysis of HEK293T cell lysate transfected with gAnkB-WT-halo (lane 1) or gAnkB-PSK-halo (lane 2) blotted with the tAnkB antibody.

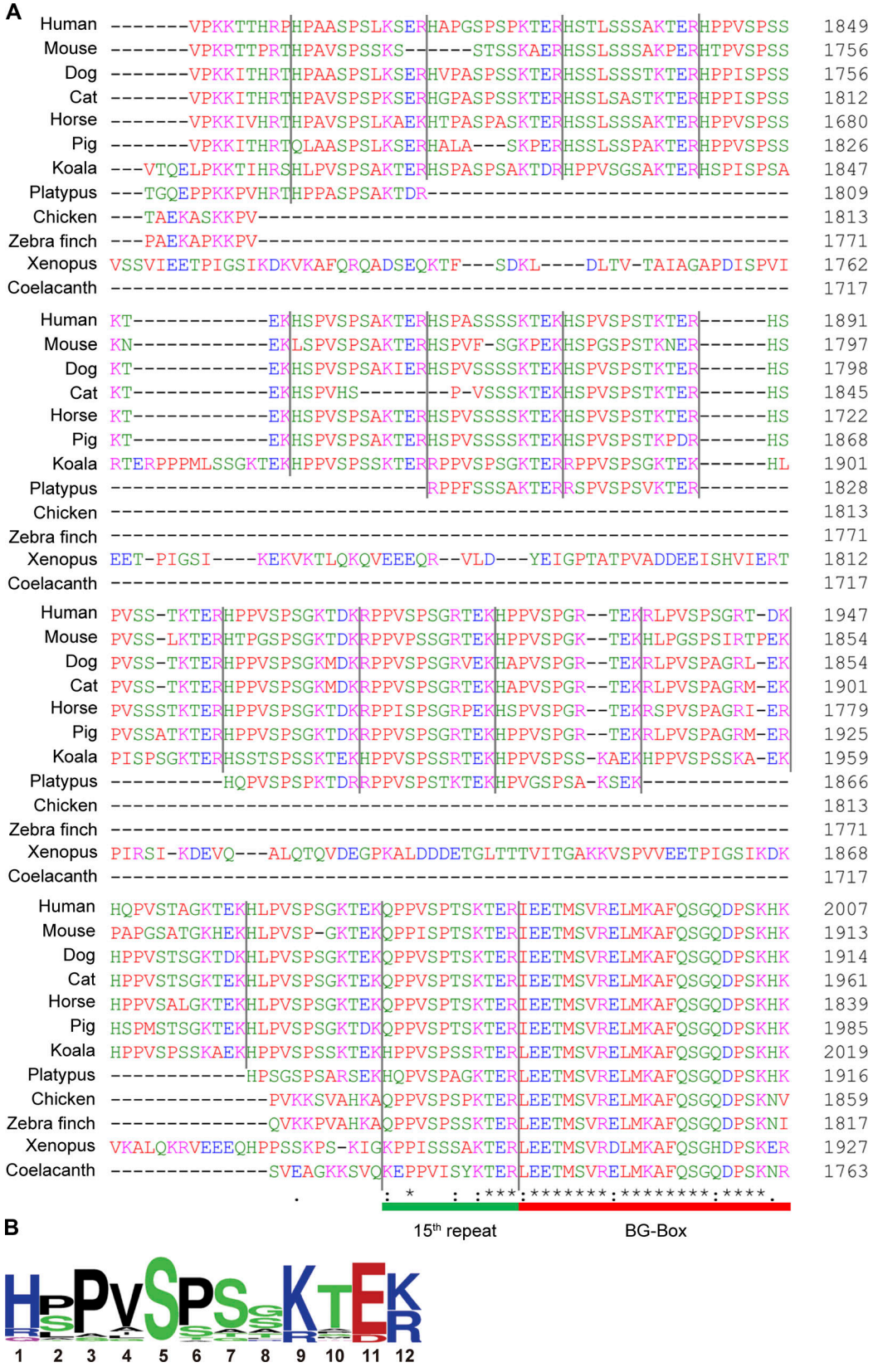

Figure S2. **The gAnkB repeated motifs are highly conserved in high vertebrates. (A)** Sequence alignment of the gAnkB 15R from different species. Boundaries of different repeats are indicated by black lines. The last repeat (the 15th repeat) is underlined in green, and one portion of the BG-box is underlined in red. *, :, and . indicate fully conserved, highly conserved, and conserved residues, respectively. **(B)** Integrated sequence logo plot of all the 15 repeats of gAnkB from human, mouse, dog, cat, horse, pig, and koala sequences. Positions of the residues in the 15 repeats are labeled below the residue.

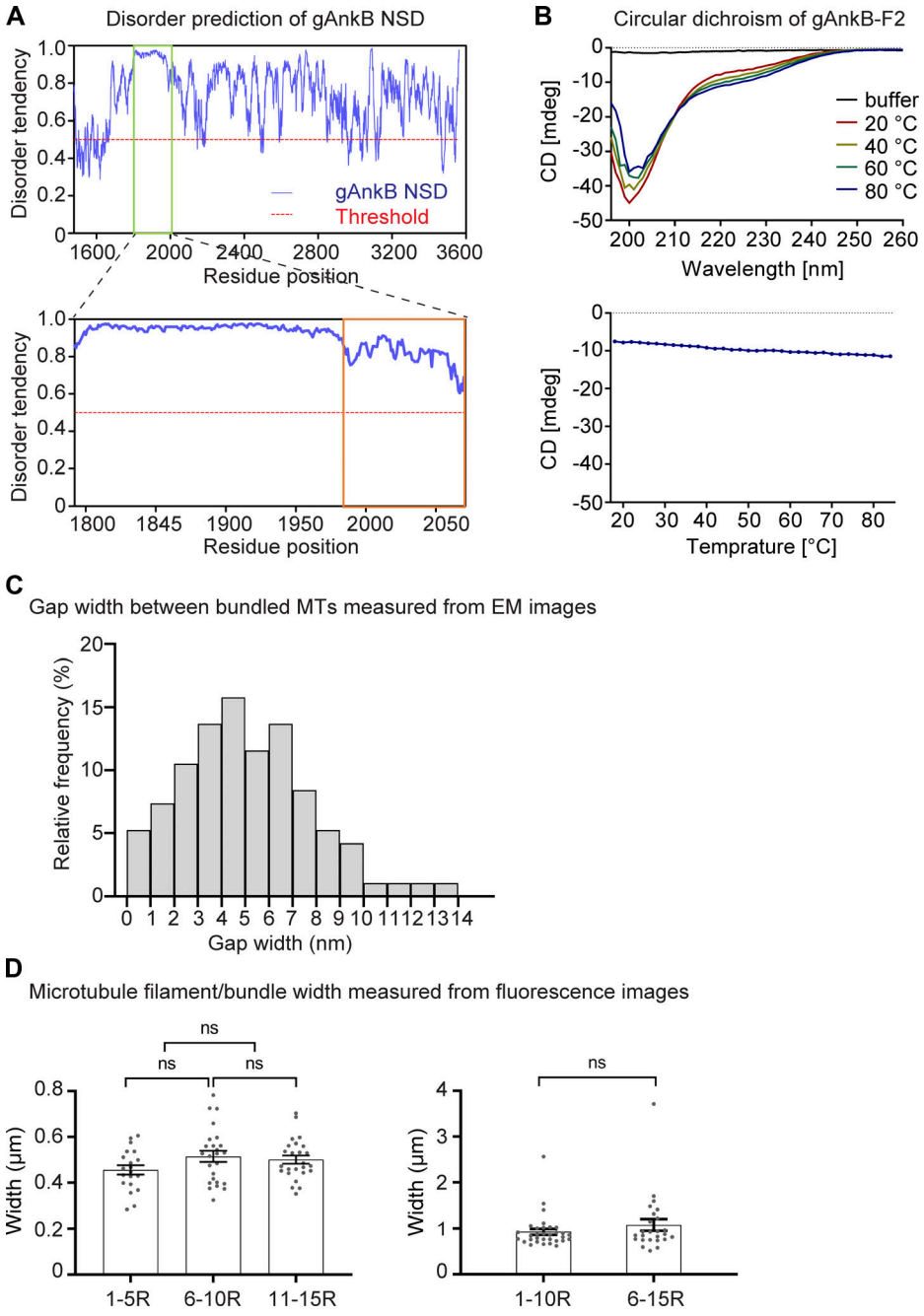

Figure S3. **The gAnkB NSD and F2 are intrinsically disordered. (A)** Disorder prediction of the entire gAnkB giant insertion (aa 1477–3561) by IUPre2A (https://iupred2a.elte.hu/). Disorder probability value in the y axis higher than 0.5 means that the region is likely to be disordered. The position of the gAnkB-F2 is boxed in green, which is expanded in the lower panel. The position of the BG-box is boxed in orange in the lower panel. **(B)** Circular dichroism spectra of gAnkB-F2 (fusion tag removed) recorded at the indicated temperatures. The ellipticities of the protein at 220 nm as a function of temperature are plotted and displayed at the bottom. **(C)** Distribution of the measured gap width between two neighboring bundled MTs in the gAnkB-F2 group in Fig. 2 F (n = 95). **(D)** Quantification of the MT filament or bundle width using fluorescence images from in vitro–imaging–based bundling assays. Left: Comparison of the MT filament or bundle width among the 1–5 repeats (1-5R), 6–10 repeats (6-10R), and 11–15 repeats (11-15R). Mean ± SEM; t test; n = 20 for 1-5R; n = 25 for 6-10R and 11-15R. Right: Comparison of the MT filament or bundle width between the 1–10 repeats (1-10R) and the 6–15 repeats (6-15R). Mean ± SEM; Mann-Whitney test; ns, nonsignificant; n = 32 for 1-10R; n = 25 for 6-15R.

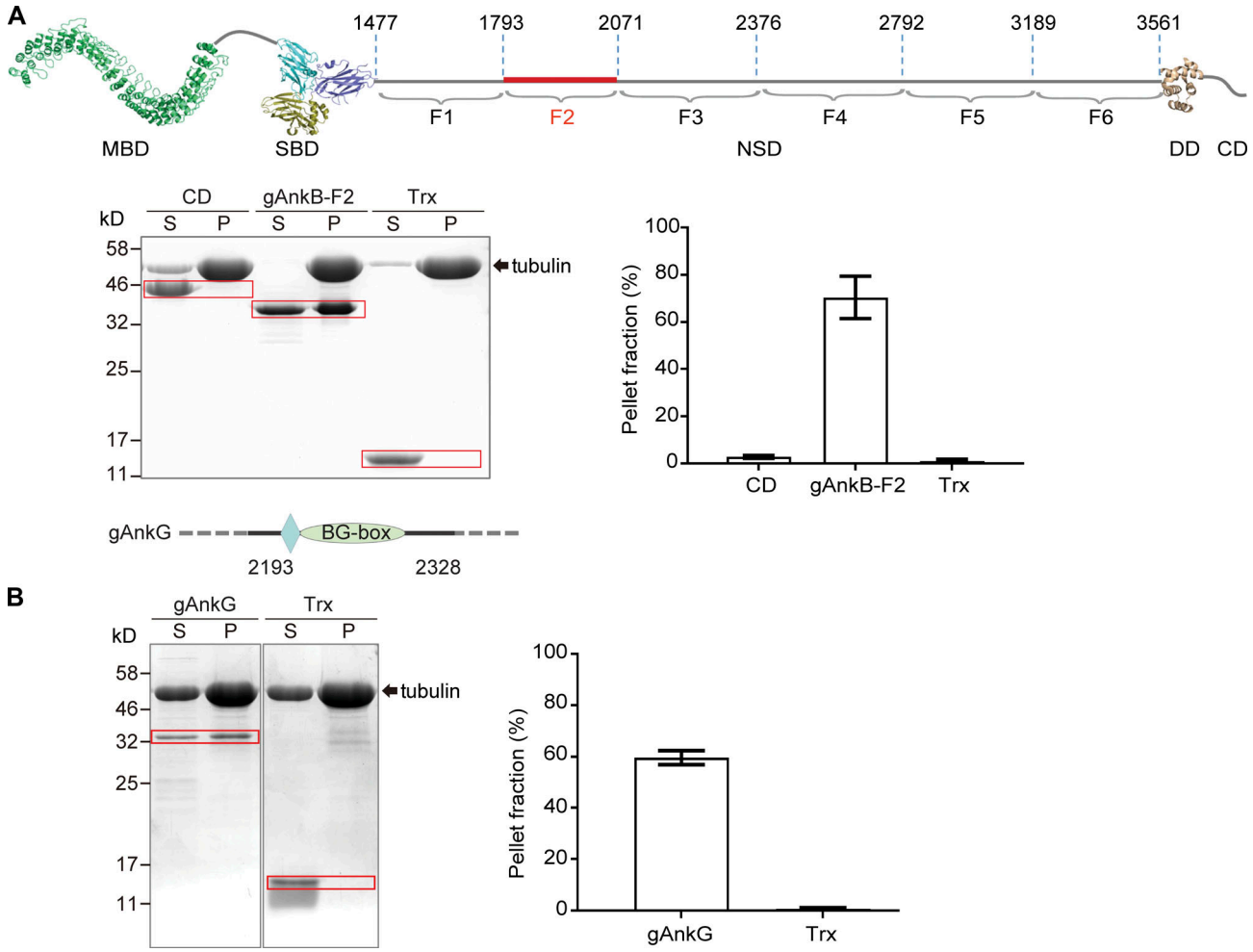

Figure S4. **The C-terminal ends of 220 kD/440 kD AnkB each contain another type of intrinsically disordered repeating sequence but does not bind to MTs. (A)** Top: Schematic of gAnkB domains including membrane binding domain (MBD), SBD, NSD, and CD (highlighted in red). Bottom left: Coomassie blue–stained SDS-PAGE gel of a MT cosedimentation experiment performed with 2 mg/ml Taxol-polymerized tubulins and indicated recombinant proteins, each at 10 µM (Trx at 30 µM). Supernatant and pellet fractions are labeled as S and P, respectively. The bands of tubulin (~55 kD) are marked by an arrow. CD, gAnkB-F2, and Trx bands are indicated with red boxes. Bottom right: The pellet fractions were quantified on the basis of band intensity and SDS-PAGE sample loading ratio (mean ± SEM; n = 3). **(B)** Top: Schematic of rat gAnkG fragment containing one 12-aa repeat and a BG-Box. Bottom left: Coomassie blue–stained SDS-PAGE gel of a MT cosedimentation experiment performed with 2 mg/ml prepolymerized tubulins and gAnkG fragment or the Trx control, each at 10 µM (Trx at 30 µM). Bottom right: The pellet fractions were quantified on the basis of band intensity and SDS-PAGE sample loading ratio (mean ± SEM; n = 3).

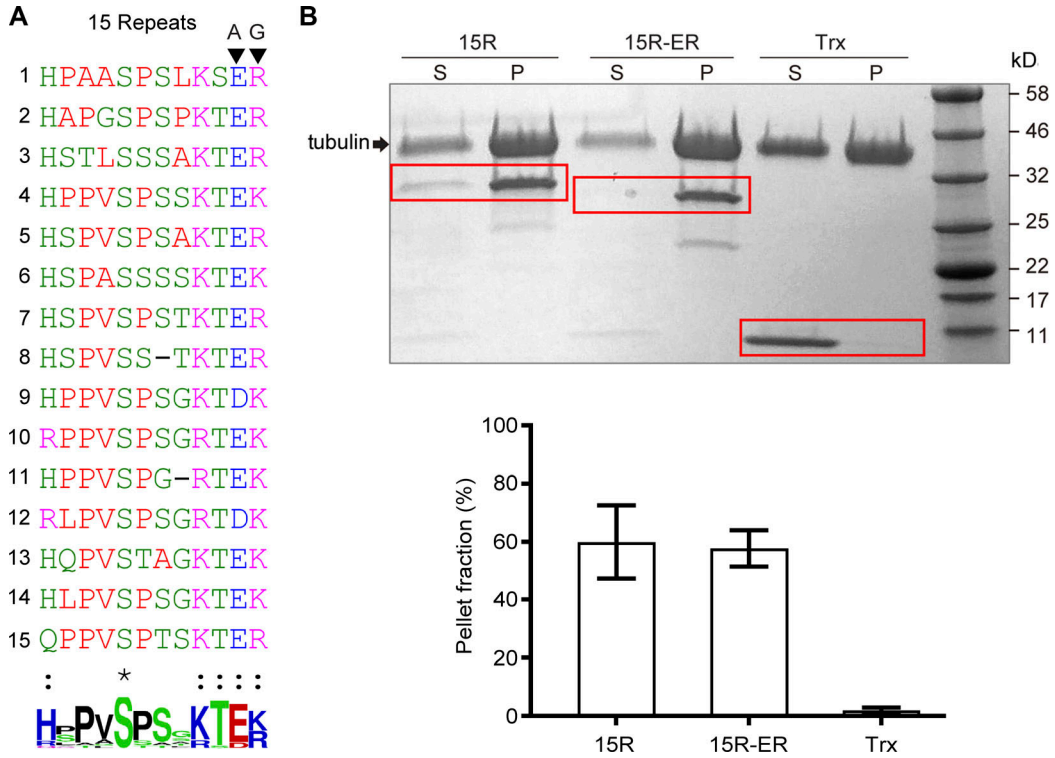

Figure S5. **Replacement of Asp/Glu-Lys/Arg at the end of each 12-aa repeat with Ala-Gly does not affect the MT binding of gAnkB. (A)** Alignment of the 15R of human gAnkB with the sequence logo plot shown beneath. Residues at the 11th and 12th positions in the 12-aa repeats, marked by black triangles, are mutated in the ER mutant of gAnkB (15R-ER). *, :, and . indicate fully conserved, highly conserved, and conserved residues, respectively. **(B)** Result of a cosedimentation assay performed with 5 µM WT human gAnkB 15R and its mutant with the last two residues (Asp/Glu-Lys/Arg) of each repeat replaced with Ala-Gly (15R-ER) and Trx as the control. All of the gAnkB proteins were Trx tagged. The bands of tubulin (~55 kD) are indicated by an arrow. gAnkB fragments and Trx bands are indicated with red boxes. The pellet fractions were quantified on the basis of band intensity and SDS-PAGE sample loading ratio (mean ± SEM; n = 3).

Video 1. **Nonaxis EB3 in WT axon.** Cultured *AB37*$^{f/f}$ *Nes-Cre*$^{-}$ hippocampal neurons were transfected with EB3-GFP and imaged at DIV4. Time-series images were taken on an axon every 3 s at 200-ms exposure time with 30% laser power of Andor XD revolution spinning disk confocal microscope (Yokogawa CSU-X1, 5,000 rpm scan head; 100×/1.4 NA oil objective). A total 2-min video was captured with MetaMorph software (Molecular Devices), and the final video was generated using Fiji software with a play speed of 20 frames/s.

Video 2. **Nonaxis EB3 in gAnkB-knockout axon.** Cultured *AB37*$^{f/f}$ *Nes-Cre*$^{+}$ hippocampal neurons were transfected with EB3-GFP and imaged at DIV4. The video was acquired with the same settings as in Video 1.

Video 3. **Invading EB3 in gAnkB-knockout filopodia.** Cultured *AB37*$^{f/f}$ *Nes-Cre*$^{+}$ hippocampal neurons were transfected with EB3-GFP and imaged at DIV4. Time-series images were taken on an axonal filopodium every 3 s at 200-ms exposure time for 2 min in total. The final video was generated at 20 frames/s.

Video 4. **Invading EB3 in WT filopodia.** *AB37*$^{f/f}$ *Nes-Cre*$^{-}$ hippocampal neurons were transfected with EB3-GFP and imaged at DIV4. The video was acquired with the same settings as in Video 3.

Video 5. **gAnkB-WT rescue nonaxis EB3.** Cultured *AB37*$^{f/f}$ *Nes-Cre*$^{+}$ hippocampal neurons were transfected with EB3-GFP together with gAnkB-WT plasmid. Time-series images were taken on an axon on DIV4 every 3 s at 200-ms exposure time for 2 min in total. The final video was generated at 20 frames/s.

Video 6. **gAnkB-PSK rescue nonaxis EB3.** Cultured *AB37*$^{f/f}$ *Nes-Cre*$^{+}$ hippocampal neurons were transfected with EB3-GFP together with gAnkB-PSK mutant plasmid. The video was acquired with the same settings as in Video 5.

Video 7. **gAnkB-PSK rescue invading EB3 in filopodia.** Cultured *AB37*$^{f/f}$ *Nes-Cre*$^{+}$ hippocampal neurons were transfected with EB3-GFP together with gAnkB-PSK mutant plasmid. Time-series images were taken on an axonal filopodium on DIV4 every 3 s at 200-ms exposure time for 2 min in total. The final video was generated at 20 frames/s.